Experimental Investigation of Projectile Integrity While Driving Through an Axisymmetric Baffled and Railed Ram Accelerator

Chase Roumain Smith

A thesis
submitted in partial fulfillment of the
requirements for the degree of

Master of Science in Aeronautics & Astronautics

University of Washington

2021

Committee:

Carl Knowlen

Bob Breidenthal

Program Authorized to Offer Degree:
Department of Aeronautics and Astronautics

University of Washington

Abstract

Experimental Investigation of Projectile Integrity While Driving Through an Axisymmetric Baffled and Railed Ram Accelerator

Chase Roumain Smith

Chair of the Supervisory Committee:
Professor Carl Knowlen
Department of Aeronautics and Astronautics

Investigations of the operational envelope of a baffled and railed axisymmetric ram accelerator occasionally yield anomalous results where large pressure spikes precede a large drop in performance. Using experimentally obtained pressure data in tandem with ANSYS structural analysis modules, Finite Element Analysis (FEA) was performed to assess the structural integrity of the ram accelerator projectile. Utilizing pressure fields from experiments, FEA indicated that the polycarbonate sub-caliber projectiles used in these tests experience plastic deformation and compromised structural integrity. Similar analysis was also conducted using a sturdier 6061 aluminum projectile which resulted in no deformation or factors of safety below 1; however, these projectiles are significantly heavier and less scientifically useful. A 2-piece shell projectile made of 7075 aluminum was then designed in order to reduce weight and maintain the increased strength of the aluminum relative to the polycarbonate. The shell style projectile showed minimal internal deformation and no external plastic deformation when subjected to the same high pressure as the polycarbonate, suggesting this projectile be used in future experiments where high pressures occur.

TABLE OF CONTENTS

Page

List of Figures ii

List of Tables viii

Chapter 1: Introduction 1

Chapter 2: Experimental Setup & Background 5
- 2.1 Experimental Setup 5
- 2.2 Ram Projectiles 11

Chapter 3: Projectile Simulation Using Experimental Data 16
- 3.1 Experimental Data 16
- 3.2 ANSYS Structural Simulation Setup 21
- 3.3 Polycarbonate Projectile Results 24
- 3.4 Aluminum Projectile Results 45
- 3.5 Shelled Projectile Results 54

Chapter 4: Discussion 60
- 4.1 Synopsis 60
- 4.2 Future Research and Testing 62
- 4.3 Conclusion 63

Bibliography 64

Appendix A: Additional Figures 67

Appendix B: Material Information 70

Appendix C: Matlab Code 73

LIST OF FIGURES

1.1 A conventional air-breathing ramjet. 2

1.2 Diagram showing the flow fields and operation of a thermally choked ram accelerator. 3

2.1 Diagram showing the setup and relative distances of components in the UW Ram Accelerator System. 6

2.2 Ram Stage 1 and Ram Stage 2. All stations 6 through 15 and the spacer insert are instrumented with pressure sensors and magnetic probes. . 7

2.3 Section view of Ram Stages 1 and 2 with BTRA500 baffle inserts in the first stage and RTRA200 rail inserts in the second stage. 8

2.4 Section view close-up of baffle inserts (left) and rail inserts (right). . 9

2.5 Drawing showing dimensions of P300 polycarbonate projectile. All dimensions in inches. 12

2.6 O101 obturator used with the P300 projectile. Constructed of polycarbonate it is used to stop launch gun gas blow by as well as aid in the starting process. The thick obturator base in positioned against the projectile base when loaded into the launch gun. 13

2.7 7075 Aluminum Shell projectile with same external dimensions as polycarbonate P300. Minimum shell thickness is 4mm or 0.158in. Connection is 4mm pitch trapezoidal acme threading. 15

3.1 Examples of a quadrapole signal (left) and a dipole signal (right) resulting from the magnet in the projectile passing quickly by the magnetic probes at stations 1 and 17. 17

3.2 Example of a pressure signal from the projectile, combustion, and obturator passing by the pressure sensor at station 13. 18

3.3 The time of the magnet passing Station 13 (left) and that same time marked on the pressure sensors signal at Station 13 (right). 19

3.4 Example of a projectile laid over the Station 13 pressure profile. . . . 20

3.5 Example project schematic as viewed from the Project Page in ANSYS Workbench. 22

3.6 HS2159: Projectile and pressure wave velocity distribution undergoing consistent acceleration. 25

3.7 Steady driving pressure overlaid on a P300 polycarbonate projectile. . 26

3.8 CFD Simulation: Gas and rail inserts travelling at 1,400m/s at inlet towards stationary projectile. Chemistry is $1.8CH_4+2O_2+7.52N_2$ at 75psi. Simulated by Navid Daneshvaran using ANSYS Fluent. 26

3.9 Safety factor resulting from steady driving acceleration on P300 polycarbonate projectile. 27

3.10 Sectioned view showing safety factor resulting from steady driving acceleration on P300 polycarbonate projectile. 28

3.11 Deformation resulting from steady driving acceleration on P300 polycarbonate projectile. 28

3.12 Section view of deformation resulting from steady driving acceleration on P300 polycarbonate projectile. 29

3.13 HS2168: Projectile and pressure wave velocity distribution with an unexplained drop in performance in the RTRA Section. 31

3.14 Unusually high pressure signals from the end of the BTRA section, just before reduced performance. 32

3.15 P10 High pressure spike overlaid on a P300 polycarbonate projectile. 33

3.16 Safety factor resulting from P10 high pressure spike on P300 polycarbonate projectile. 34

3.17 Section view of safety factor resulting from P10 high pressure spike on P300 polycarbonate projectile. 34

3.18 Deformation resulting from P10 high pressure spike on P300 polycarbonate projectile. 35

3.19 Section view of deformation resulting from P10 high pressure spike on P300 polycarbonate projectile. 36

3.20 Transient Simulation. Safety factor resulting from P10 high pressure spike on P300 polycarbonate projectile. 36

3.21 Transient Simulation. Section view of safety factor resulting from P10 high pressure spike on P300 polycarbonate projectile. 37

3.22 Transient Simulation. Deformation resulting from P10 high pressure spike on P300 polycarbonate projectile. 37

3.23 Transient Simulation. Section view of deformation resulting from P10 high pressure spike on P300 polycarbonate projectile. 38

3.24 Ptrin High pressure spike overlaid on a P300 polycarbonate projectile. 40

3.25 Safety factor resulting from Ptrin high pressure spike on P300 polycarbonate projectile. 41

3.26 Section view of safety factor resulting from Ptrin high pressure spike on P300 polycarbonate projectile. 41

3.27 Deformation resulting from Ptrin high pressure spike on P300 polycarbonate projectile. 42

3.28 Section view of deformation resulting from Ptrin high pressure spike on P300 polycarbonate projectile. 42

3.29 CFD Simulation: Gas and rail inserts travelling at 1,200m/s at inlet towards stationary projectile. Chemistry is $1.8CH_4+2O_2+7.52N_2$ at 75psi. Simulated by Navid Daneshvaran using ANSYS Fluent. 43

3.30 Safety factor resulting from steady driving acceleration on P300 aluminum projectile. 46

3.31 Section view of safety factor resulting from steady driving acceleration on P300 aluminum projectile. 46

3.32 Deformation resulting from steady driving acceleration on P300 aluminum projectile. 47

3.33 Section view of deformation resulting from steady driving acceleration on P300 aluminum projectile. 47

3.34 Safety factor resulting from P10 high pressure spike on P300 Aluminum projectile. 48

3.35 Section view of safety factor resulting from P10 high pressure spike on P300 Aluminum projectile. 49

3.36 Deformation resulting from P10 high pressure spike on P300 Aluminum projectile. 49

3.37 Section view of deformation resulting from P10 high pressure spike on P300 Aluminum projectile. 50

3.38 Safety factor resulting from Ptrin high pressure spike on P300 Aluminum projectile. 51

3.39 Section view of safety factor resulting from Ptrin high pressure spike on P300 Aluminum projectile. 52

3.40 Deformation resulting from Ptrin high pressure spike on P300 Aluminum projectile. 52

3.41 Section view of deformation resulting from Ptrin high pressure spike on P300 Aluminum projectile. 53

3.42 Safety factor resulting from P10 high pressure spike on P300 shell projectile. 55

3.43 Section view of safety factor resulting from P10 high pressure spike on P300 shell projectile. 55

3.44 Deformation resulting from P10 high pressure spike on P300 shell projectile. 56

3.45 Section view of deformation resulting from P10 high pressure spike on P300 shell projectile. 56

3.46 Safety factor resulting from Ptrin high pressure spike on P300 shell projectile. 57

3.47 Section view of safety factor resulting from Ptrin high pressure spike on P300 shell projectile. 58

3.48 Safety factor resulting from Ptrin high pressure spike on P300 shell projectile. 59

3.49 Section view of safety factor resulting from Ptrin high pressure spike on P300 shell projectile. 59

A.1 Dimensions between each of the stations along the ram test section. . 67

A.2 Safety factor resulting from P13 on P300 shell projectile. 68

A.3 Section view of safety factor resulting from P13 on P300 shell projectile. 68

A.4 Deformation resulting from P13 on P300 shell projectile. 69

A.5 Section view of deformation resulting from P13 on P300 shell projectile. 69

B.1 6061-T6 Aluminum Properties, information provided by Gabrain International Ltd. 71

B.2 7075-T6 Aluminum Properties, information provided by Gabrain International Ltd. 72

LIST OF TABLES

3.1 Configuration and shot details for HS2159. 24

3.2 Configuration and shot details for HS2168. 30

ACRONYMS

BTRA Baffle Tube Ram Accelerator

CAD Computer Aided Design

CFD Computational Fluid Dynamics

DAQ Data Acquisition System

EM Electromagnetic

FEA Finite Element Analysis

HARP High Altitude Research Project

PC Polycarbonate

RTRA Rail Tube Ram Accelerator

TCRA Thermally Choked Ram Accelerator

UW University of Washington

ACKNOWLEDGMENTS

First, I would like to thank and acknowledge my advisor: Professor Carl Knowlen. Without whom I would have never listened to hours of stories detailing the history, trials, and tribulations of ram wherein pearls of wisdom constantly laid.

I would also like to extend my gratitude to the PhD students: Brian, who took me from an ignorant visitor to experienced experimenter, damage assessor, and tube assembler. Navid, who assisted as I dipped my toes (and fell in) to different parts of the simulation world.

A hearty thanks the undergraduate volunteers and independent study'ers of the lab, without whom I would have had to turn many more wrenches.

Finally I would like to thank my family, friends, and loved ones who kept me sane during the wild, strange, and stressful time that has been the past 2 years.

Chapter 1

INTRODUCTION

The University of Washington (UW) ram accelerator is a mass driver designed to bring a projectile to supersonic and hypersonic velocities in order to creatively solve a variety of challenges in reaching both space and the depths of the earth. This study will focus on research leading to the development of the space launch applications of this technology. The current technique for delivering payloads to space is using a rocket: a vehicle which has taken men to the moon and instrument carrying spacecraft beyond. However, the severe drawback of using a rocket launch for payload delivery is the immense amount of fuel required to reach orbit, making this method incredibly costly at $\$10,000$/lb of payload [1]. Additionally rockets are almost exclusively single use vehicles which means the frequency of their use is limited by availability of resources and manufacturing hours.

One notable attempt to reach space without a rocket is Project HARP. The High Altitude Research Project was a joint effort between the United States Department of Defense and the Canadian Department of Defense in 1961 to reach space using a ground based canon [2]. While ultimately unsuccessful as a space launch technology, the project very successfully tested prototype gun-launched rockets and aerospace vehicle performance at high altitude. There are several driving reasons behind why project HARP and similar projects did not get off the ground; the primary reason being how the projectile is accelerated in a conventional gun. At the most simple level, gun-based experiments involve pushing a projectile down a barrel using a gas pressure gradient, most commonly by igniting a fast burning fuel. As the projectile moves down the barrel, the expanding gas behind it must match the projectiles velocity in order to

create a sustained pressure gradient. This means that at sea level, by the end of the gun's barrel, the gas behind the projectile has to travel from a zero velocity to around 9.4 km/s for direct launch to orbit applications [2]. Thus, this technology ends up in a similar place as a rocket: a gun-based launch system has to use a significant portion of its fuel to "carry" fuel along with the projectile. It is clear that a vehicle traveling to space while carrying its payload and the extra weight of fuel creates ballooning expenses and limitations. This is avoided by use of a ram accelerator, where the delivery vehicle accelerates as it passes through a stationary fuel, requiring only that the vehicle carry its payload as well as the resources for orbit circularization and other mission tasks.

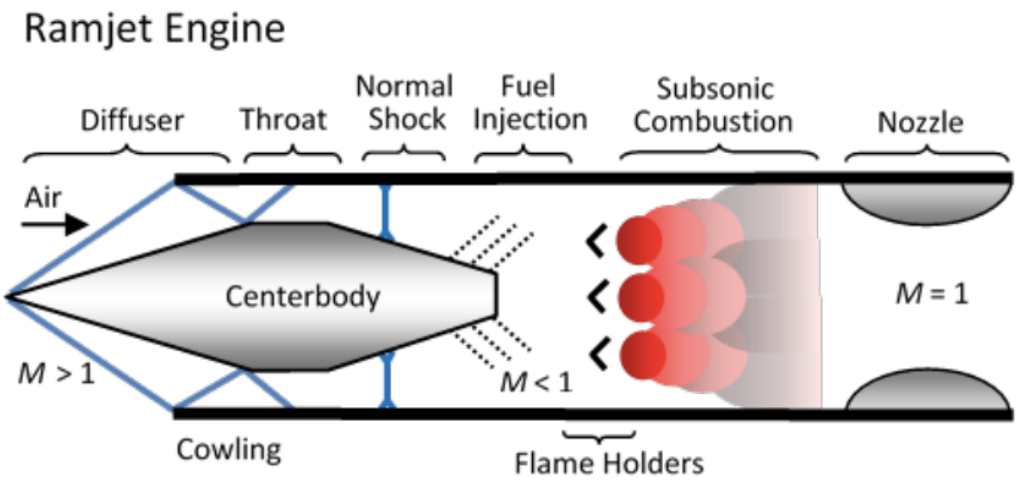

Figure 1.1: A conventional air-breathing ramjet.

A ram accelerator operates similarly to a conventional air-breathing ramjet used on aircraft such as the famous SR-71 Blackbird. In a ramjet, supersonic air flows around a supersonic diffuser and into a throat where it is decelerated to subsonic speeds as shown in Figure 1.1. Fuel is then injected and ignited causing subsonic combustion. The combustion products then expand, pushing out of a nozzle where

they accelerate from subsonic to supersonic. The combusted fuel-air products exit at higher velocity and pressure than the air at the engine's inlet, resulting in thrust generation.

A ram accelerator works on the same principle as the ramjet. The projectile, or "engine", is shot at supersonic speeds through a tube of mixed fuel and oxidizer where a system of shocks in the supersonic diffuser and throat slow the incoming mixture to subsonic. This system of shocks has the additional benefit of preheating the propellant to facilitate subsonic combustion near the base of the projectile as shown in Figure 1.2. The acceleration of the propellant as it combusts leads to thermal choking where the gas transitions from subsonic to sonic. The high pressure between the shock system and the thermally choked region results in thrust that accelerates the projectile. This mode of operation is known as a thermally choked ram accelerator and is the mode of concern in this study [3] [4].

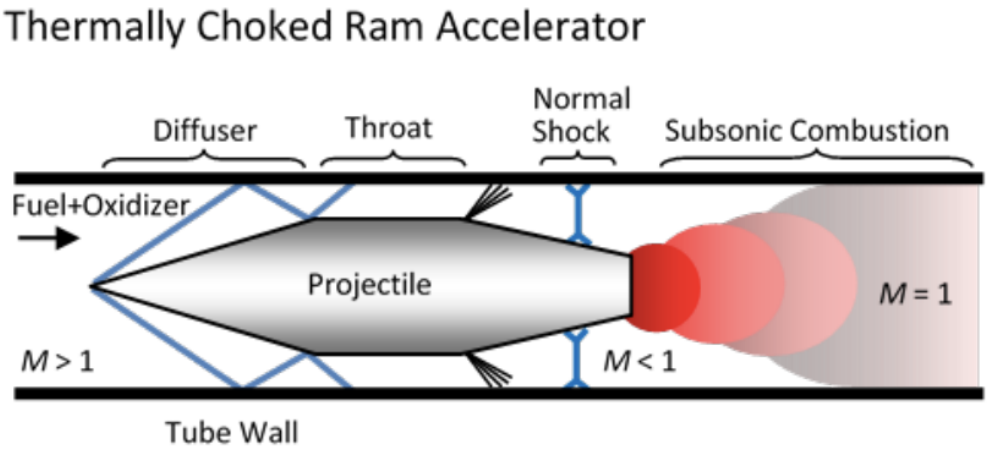

Figure 1.2: Diagram showing the flow fields and operation of a thermally choked ram accelerator.

Experimentally, ram accelerators have demonstrated successful operation in many configurations; however, on occasion there are enigmatic drops in performance. Often a drop in performance indicates that a limitation is being reached in the system: for example, the gasdynamic limit of a certain chemistry will experience reduced performance at a high enough velocity as drag begins to equal thrust [5][6]. Yet at higher pressures it is unclear if these drops in performance are the result of a limitation or if they are a result of the structure of the projectile being compromised. This study seeks to determine if the projectiles used in the UW Ram Lab experiments maintain structural integrity throughout experimental runs and to assess the reliability of other projectile configurations.

Chapter 2

EXPERIMENTAL SETUP & BACKGROUND

2.1 Experimental Setup

The University of Washington Ram Lab's mass driver is a system designed to launch projectiles at supersonic velocities into a ram test section where experiments are conducted and then safely slowed and stopped. There are 7 main steps to the projectile's journey throughout each experimental run.

1. The projectile and obturator are launched from a helium light gas gun by pressurizing a breech region until scored aluminum diaphragms burst, releasing helium and propelling the projectile and obturator forward.

2. The obturator blocks blow-by of gun propellant (helium) and pushes the projectile as they accelerate through the launch tube.

3. The helium vents into a gun muzzle dump tank via perforations in the launch tube. Magnetic and pressure sensors at the exit of the launch tube detect the projectile passing.

4. The projectile and obturator enter the first ram stage where starting occurs (this mechanism is discussed in Section 2.1.2) and the ram accelerator propulsive mode is established. The obturator is pushed back as pressure builds up between it and the projectile. Magnetic and pressure sensors gather data throughout the shot duration.

5. The second stage in entered, continued acceleration. Magnetic and pressure sensors gather data throughout.

6. The projectile and obturator drift through the remaining sections of evacuated tube. Instrumentation at the beginning of the evacuated tube provide high resolution data for exit velocity validation.

7. The projectile and obturator pass into the final dump tank allowing the gasses to expand. Both pieces are stopped in a dense roll of carpet backed by a 2 inch steel block and a 5 inch aluminum block

Figure 2.1 shows a diagram of the full experimental setup with the distances of each section. This investigation will focus on what occurs in the ram stages rather than during launch or deceleration.

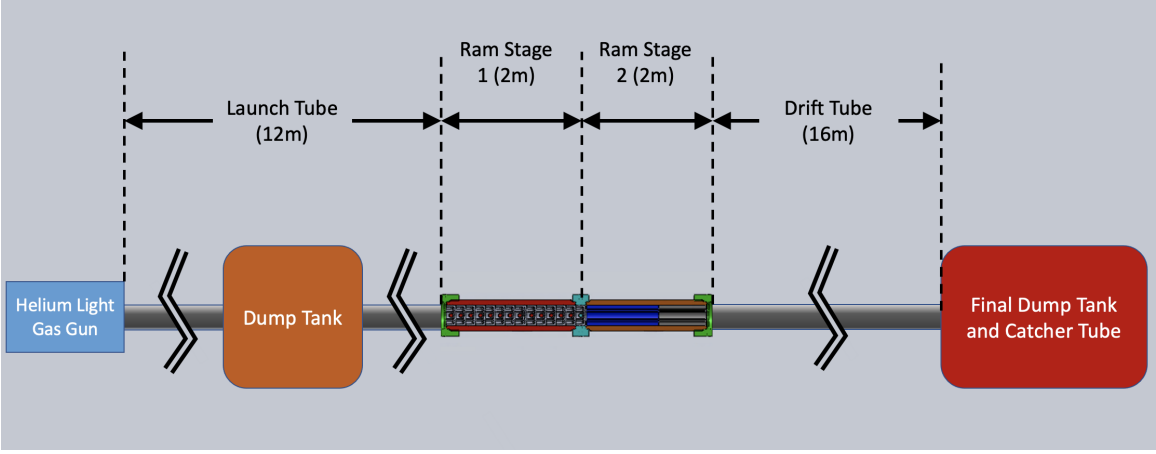

Figure 2.1: Diagram showing the setup and relative distances of components in the UW Ram Accelerator System.

There are 11 stations along the ram test section, each station contains 2 port holes opposite each other. The top ports are used for magnetic probes that were designed and constructed in-house at the UW Ram Lab [7]. These probes are used to detect

the magnets embedded within the projectile as it passes by. Opposite the magnetic probes, piezoelectric pressures sensors are mounted that monitor static pressure near the tube wall as the projectile and obturator pass by. Each station is numbered as shown in Figure 2.2; the connecting region between the two ram stages is referred to as the "spacer insert" and is a station instrumented the same as each of the stations along the stages. Station spacing can be found in Appendix A Figure A.1. Though not shown in either Figures 2.1 or 2.2, the helium light gas gun, launch tubes, ram stages, and drift tubes are all bolted together with a series of threaded steel flanges that ensure longitudinal compression and a good seal.

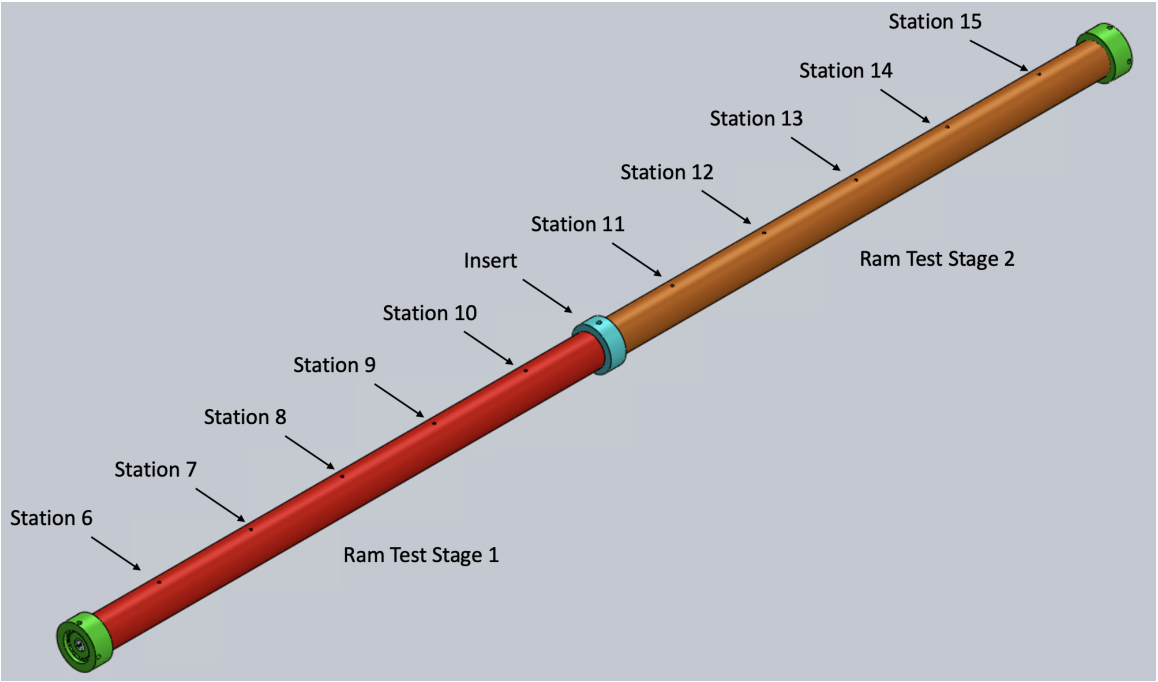

Figure 2.2: Ram Stage 1 and Ram Stage 2. All stations 6 through 15 and the spacer insert are instrumented with pressure sensors and magnetic probes.

2.1.1 Internal Configurations: Tube Inserts

Each of the ram stages consists of:

- Shell Tubes: a 3/4" thick-walled steel tube that houses the inserts. The instrumentation ports are machined into the shell tubes that are designed to withstand the large pressures resulting from combustion. (Red and orange in Figure 2.3)

- End Caps: screwed onto the ends of the shell tubes, the end caps restrict any sliding of the inserts inside the tubes and bear the brunt of any longitudinal load. They also are the surface where diaphragms seal the tube ends to hold pressure in each stage. (Green in Figure 2.3)

- Spacer Insert: pressed between the two shell tubes, it can serve to connect the two stages into one continuous stage or two separate stages by using a diaphragm. This allows the use of different fuel+oxidizer mixtures in each stage. (Cyan in Figure 2.3)

- Baffle and Rail Inserts: interchangeable internal tube geometries used to optimize performance. (Gray, blue, and yellow in Figure 2.3)

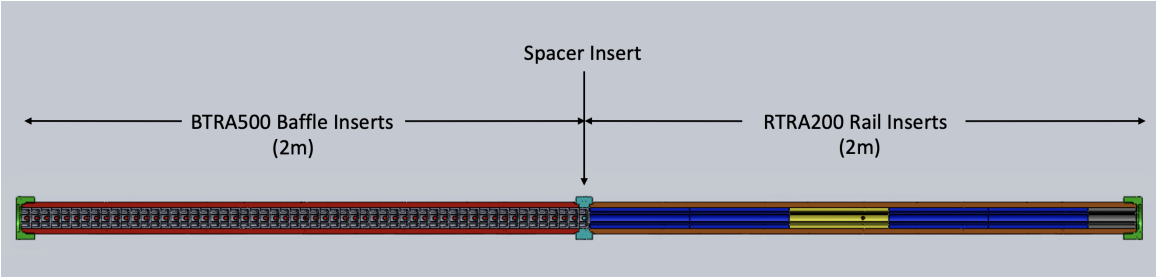

Figure 2.3: Section view of Ram Stages 1 and 2 with BTRA500 baffle inserts in the first stage and RTRA200 rail inserts in the second stage.

Rail inserts are one of the simplest internal geometries for an axisymmetric ram accelerator. They have an external diameter of 3.005in with rails that protrude radially inward to support the projectile as it travels through the section. The inner diameter of of these rails is 1.505in which guide the subcaliber projectiles down the stage. A detailed section view of the rail inserts used can be seen on the right in Figure 2.4.

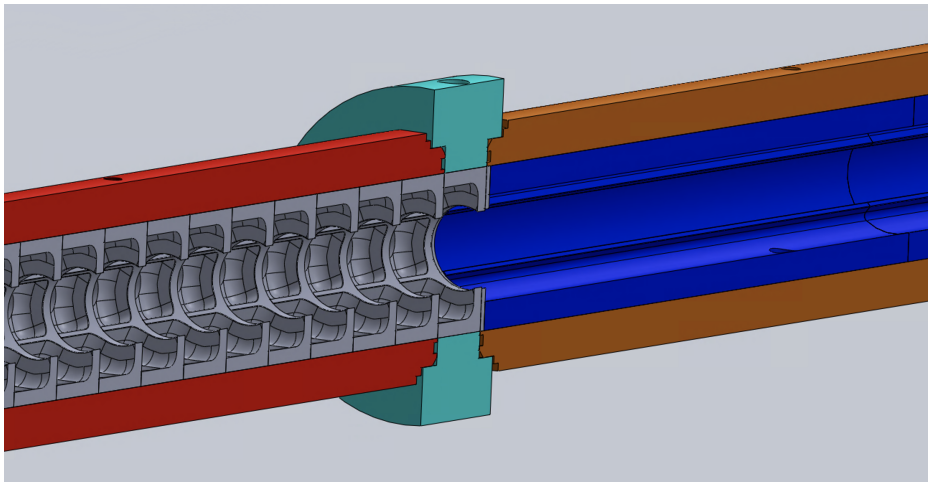

Figure 2.4: Section view close-up of baffle inserts (left) and rail inserts (right).

Baffle tube inserts are of a similar design to the rail tube in that they have the same external diameter and the same rail configuration; however, at every 1.406in along the wall there is an annulus that forms a baffle chamber as shown on the left in Figure 2.4. The volume of the baffle inserts' chambers enable the projectile to start in the ram stages at lower velocities and theoretically can triple thrust at a given fill pressure [8]. The specific design of the baffles has gone through several iterations with testing involving both a "washer like" baffle [9] and inclined baffles [10] where the baffle chamber tapers inward from one side. The current iteration of baffles shown in Figure 2.4 are a washer style baffle with a filet at the base adding more structure and making them easier to manufacture. The design of the baffle is such that at least

one chamber is entirely obscured as a projectile with a shoulder length at least one tube caliber long passes. Obscuring the baffle serves to create a barrier that aids in keeping the high pressure combustion region from moving up the projectile body which can lead to unstart.

2.1.2 Starting & Unstarting

Starting and unstarting are two of the four processes which can occur when a projectile travels through the ram test stages. The first, and least exciting, event that can take place is supersonic coasting. This commonly occurs if the fuel+oxidizer mixture is not energetic enough, leading to the combustion wave being nonexistent or falling off the projectile base. A successful start is achieved when supersonic flow is maintained throughout the supersonic diffuser and combustion stabilizes on the base of the projectile [11]. After a successful start several things can occur to stop the projectile from continuing to accelerate down the tube. A sonic diffuser unstart occurs when there is subsonic flow in the diffuser, this creates a high pressure region in front of the projectile slowing it. A wave unstart occurs when the shock systems moves forward on the projectile until it moves ahead of the nose cone where it causes rapid deceleration of the projectile; the high pressure "wave" of the shock system and combustion then moves down the tube ahead of the projectile [11]. For the sake of this study "starting" and "start" will refer simply to the process described above and "unstarting" and "unstart" will specifically refer to the wave unstart process.

2.2 Ram Projectiles

A large number of finned projectile configurations have been tested within the ram accelerator at UW: polycarbonate, aluminum, magnesium, and titanium of different dimensions and combinations have been tested successfully. Many Ram Lab theses have been devoted to the task of testing performance of different projectile geometries and materials such as those conducted by masters student Tim Elder [12] who studied the operational window of polycarbonate projectiles, or Thomas Imrich [13] who studied projectile geometries effect of performance.

In transitioning from a smooth bore ram accelerator to an axisymmetric rail and baffled tube ram accelerator, a number of additional studies were performed where fin-less axisymmetric projectiles were developed. Through a combination of theoretical calculation, simulation, and testing the geometry and performance of different polycarbonate projectiles was tested in BTRA [14][15]. These studies involved the design and manufacture of the sub caliber P300 projectile that has been used in the majority of the last 150+ experiments.

2.2.1 Polycarbonate Projectile

The P300 projectile used is constructed of polycarbonate (PC): a light-weight strong plastic used commonly in bulletproof glass, helmets, and car lights [16]. Polycarbonate, sometimes known by one of its brand names: Lexan, is a lightweight thermoplastic ($1.2 g/cm^3$) containing carbonate groups that add structure and strength to its otherwise polymer structure. It is naturally flame retardant and maintains its strength from -20°C to 140°C [16]. PC has a tensile yield strength of 65MPa or around 10ksi depending on how it is created and will elongate 6-7% at yield [16]. These projectiles are machined from a rod of polycarbonate on a lathe to the dimensions shown in Figure 2.5.

The different parts of the projectile will be referred to as follows: the "nose" or "head" of the projectile refers to the conical section which points into the flow of gas, the "body" or "neck" is the cylindrical section following the nose, the "tail" is the tapered section following the body, and the "base" is the flat circular section at the end of the projectile. Additionally the "front shoulder" and "rear shoulder" refer to the sharp transitions between the head and body, and body and tail respectively. Note the bore hole in the base of the projectile that extends to just past the rear shoulder. This is where a strong magnet is secured in place by a nylon plug threaded into the base of the projectile in order to give a signal to the magnetic probes at each station.

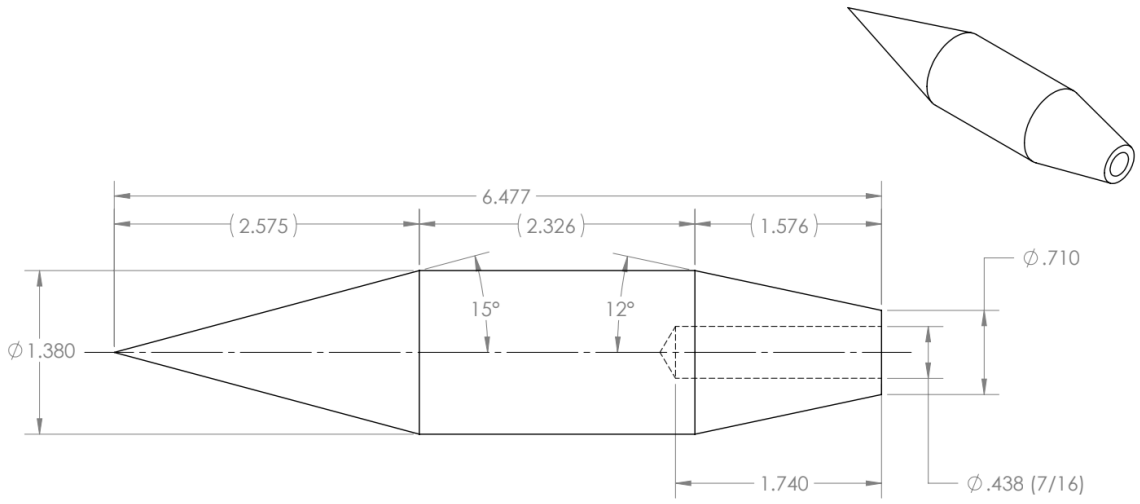

Figure 2.5: Drawing showing dimensions of P300 polycarbonate projectile. All dimensions in inches.

The polycarbonate projectiles offer many benefits but are structurally less sound than their metallic counterparts. The current P300 projectiles weight approximately 123g by themselves and 146g with the polycarbonate obturator (Figure 2.6) attached, making the task of launching them into ram sections at velocities up to 1100m/s

easily and safety achievable with light gas gun pressures below 5000psi. The light weight also allows experiments to probe larger velocity and Mach ranges at relatively safe pressures in the test sections. However, the light weight comes at the cost of a relatively low tensile strength. As mentioned earlier, there is strong evidence of projectile structural degradation that could be leading to losses in performance.

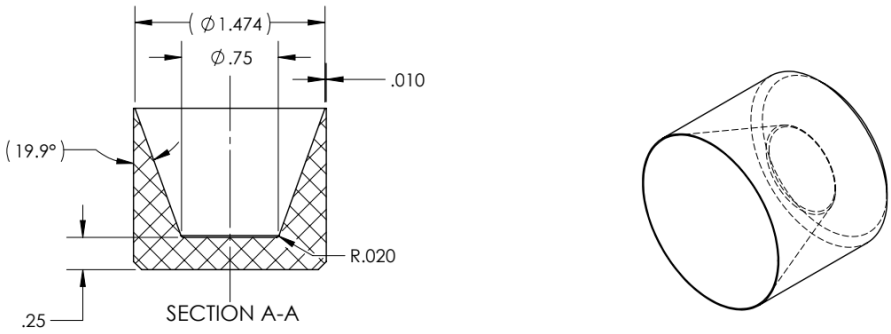

Figure 2.6: O101 obturator used with the P300 projectile. Constructed of polycarbonate it is used to stop launch gun gas blow by as well as aid in the starting process. The thick obturator base in positioned against the projectile base when loaded into the launch gun.

2.2.2 6061 Aluminum Projectile

Evidence that the polycarbonate projectile may be too weak for some ram accelerator environments requires the use of a stronger material for the projectile. Finned aluminum projectiles were commonly used for experiments in smooth bore ram accelerators, and would be used in BTRA if it were not for the density of polycarbonate being half of aluminum. These projectiles are built to the same dimensions as the polycarbonate P300, see Figure 2.5, but are made out of 6061 Aluminum. Aluminum P300s weigh 266g, 289g with the polycarbonate obturator, and have a density of 2.7g/cm^3. Their tensile yield strength is much higher than the PC at around 267MPa

or 40ksi (Appendix B Figure B.1). During experimentation they have yet to show indication of deformation or degradation while undergoing acceleration in the ram stages; however, they are twice the weight of their polycarbonate counterparts and as such the helium light gas gun used for launching the projectiles can only get these up to around 800m/s. This limits the Mach/velocity range they can explore and therefore fundamentally limits what can be learned using them.

2.2.3 Aluminum Shell Projectile

The problem of weight versus strength can be solved by keeping the exterior hard shell of aluminum but removing interior redundant mass. This allows the projectile to be launched up to 1000m/s while helping to maintain structural integrity throughout operation. To meet this requirement a projectile was designed to:

- Have the exact same exterior dimensions as the P300 projectile.
- Stay underneath 180g with a polycarbonate obturator; the maximum mass that can be accelerated to 1000m/s by the helium light gas gun.
- Carry a magnet retained by a threaded nylon rod.
- Not permanently deform during operation.

After several design iterations the final aluminum shell projectile was selected that would be tested against both the polycarbonate and 6061 aluminum projectiles. The shell projectile designed is made of the slightly stronger 7075-T6 aluminum, which has a tensile yield strength of 572MPa or 83ksi and a slightly heavier mass of 2.8g/cm^3 (Appendix B Figure B.2). The projectile weight is 153g without the obturator, 176g with the obturator, and is robust to large spikes in pressure along the body. Figure 2.7 shows a drawing of the projectile, which consists of two halves that are threaded together via trapezoidal acme threads on the inside and outside of the projectile's

shell. This design frees up the internal space to be hollow and allows easier machining that alternative methods of connection. For the purpose of simulation the threading adds a large computational load and as a result the model was simplified to a flat connecting surface on each side of the shell.

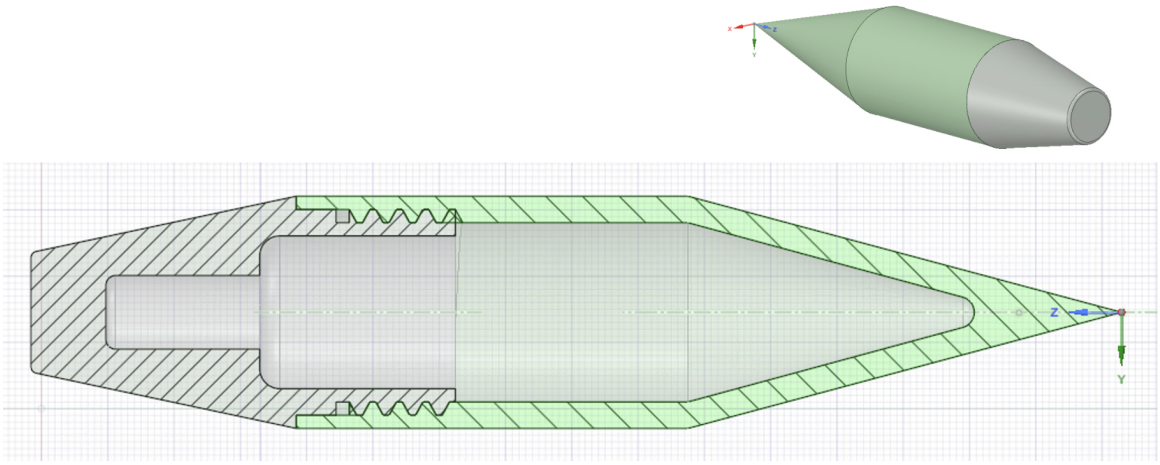

Figure 2.7: 7075 Aluminum Shell projectile with same external dimensions as polycarbonate P300. Minimum shell thickness is 4mm or 0.158in. Connection is 4mm pitch trapezoidal acme threading.

Chapter 3

PROJECTILE SIMULATION USING EXPERIMENTAL DATA

The nature of the Ram lab accelerator in its current configuration and testing regime results in extremely high forces on the projectile that result in accelerations up to $15,000+$ g [17][18]. This prohibits the possibility of instrumenting projectiles as the instrumentation would not survive long enough to convey any pertinent information, which begs the question: how can we experimentally determine what the projectile experiences?

3.1 Experimental Data

As mentioned earlier data is gathered in the ram stages in two ways: at 11 total stations through the 4m test section, there are piezoelectric pressure sensors as well as magnetic probes. The signals collected by the magnetic probes are used to determine the the times when the projectile passes by each station throughout the tube, while the pressure sensors measure the change in pressure at the tube wall. Using a combination of pressure sensor and magnetic probe data it is possible to generate a data set that correlates pressures to certain locations on the projectile.

3.1.1 Magnetic Probe and Pressure Sensor Data

The magnetic probes used throughout the ram test sections are wall mounted non-magnetic casings containing a coil normal to the tube axis developed at the University of Washington [7]. At the simplest level the magnetic probes are a solenoid attached to a multiplexor whose output is them processed using the Ram Lab DAQ. As the projectile passes, the magnet embedded within the projectile will generate current in each sensor resulting in either a dipole or quadrapole signal as shown in Figure 3.1. By locating the center of this signal it is possible to determine the time at which the magnet within the projectile passes directly beneath the probe. Using these times, and known tube dimensions, a projectile velocity distribution over the course of the two Ram Stages can be generated.

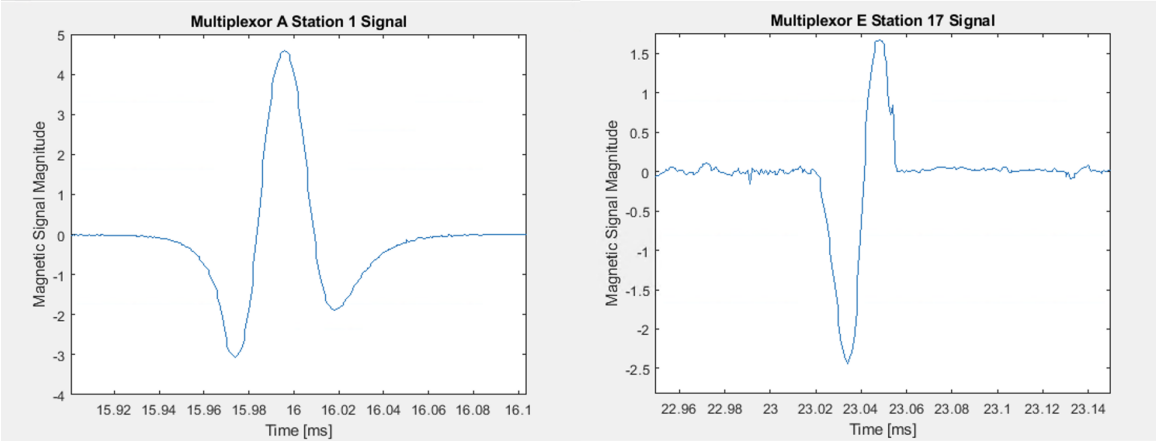

Figure 3.1: Examples of a quadrapole signal (left) and a dipole signal (right) resulting from the magnet in the projectile passing quickly by the magnetic probes at stations 1 and 17.

The pressure sensors used throughout the ram test sections are Model 119B11, B12 pressure sensors purchased from PCB Piezotronics. These sensors are mounted opposite the magnetic probes at each station and are, at the most basic level, a crystal attached to a wire; when the crystal is compressed it generates a current which is converted to a voltage that is recorded using the Ram Lab DAQ. The result is a profile of the pressure waves and shocks that propagate to the wall as the projectile passes by, as well as the pressures resulting from combustion taking place in front of, on, or aft of the projectile. An example of a pressure profile is shown below in Figure 3.2. Each PCB sensor comes with a manual that instructs the user how to convert the signal readouts collected into pressures in psi, this process has been done for each plot shown here.

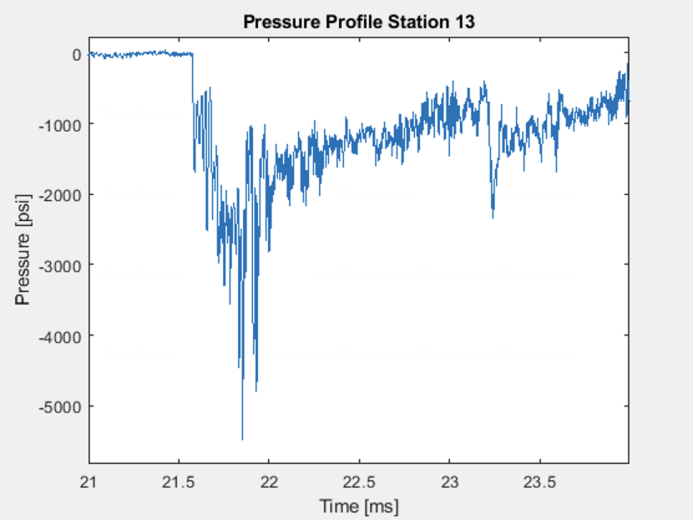

Figure 3.2: Example of a pressure signal from the projectile, combustion, and obturator passing by the pressure sensor at station 13.

3.1.2 Data Processing

The EM and pressure sensors therefore provide a time that the projectile is present at a certain station in the ram stages and its position relative to the pressure data at the same station. An example of this is shown in Figure 3.3.

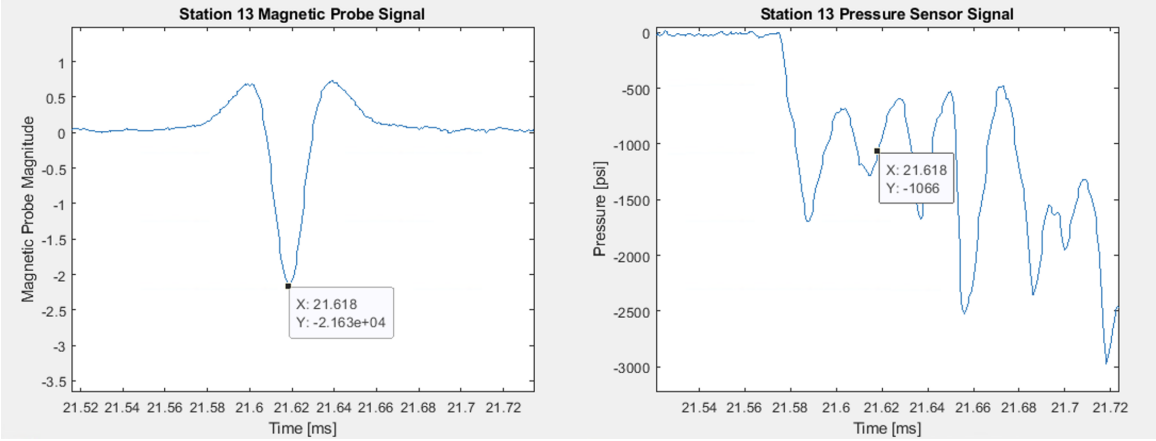

Figure 3.3: The time of the magnet passing Station 13 (left) and that same time marked on the pressure sensors signal at Station 13 (right).

Using the velocity of the projectile and knowing its physical dimensions it is possible to determine the times where the tip and tail of the projectile pass the station using Equations 3.1 shown below. Using t_{tip}, t_{tail}, and total length the pressure profile can then be "laid" over the projectile (Figure 3.4).

$$t_{tip} = \frac{1}{v}(v \times t_m - d_{tip}), \quad t_{tail} = \frac{1}{v}(v \times t_m + d_{tail}), \tag{3.1}$$

v = Velocity, t_m = Magnet Time, d_{tip} = Dist. to Tip, d_{tail} = Dist. to Tail

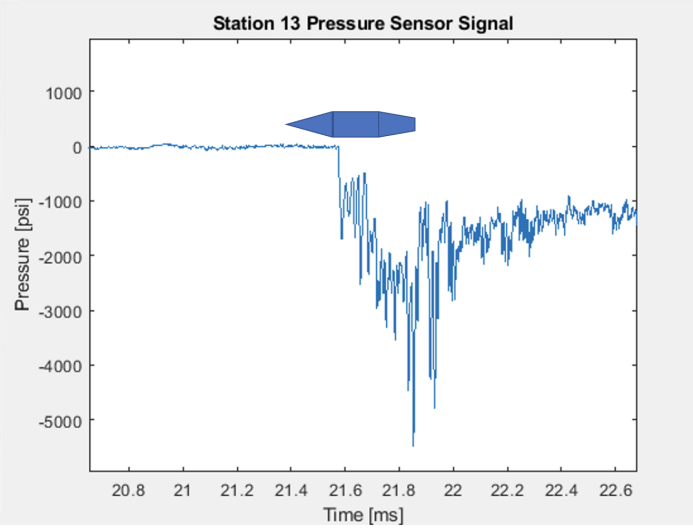

Figure 3.4: Example of a projectile laid over the Station 13 pressure profile.

Finally, the pressure data points are stepped through one by one and each point can be correlated to a position axially along the projectile resulting in a $2 \times n$ array of axial coordinate and pressure which is then exported to a .csv file for simulation use.

3.2 ANSYS Structural Simulation Setup

In order to determine the structural effects of applying pressure on the projectiles in question, simulation software must be used. The simulation software used in this study is the Static Structural and Transient Structural modules available within ANSYS Workbench. These modules used in tandem with the External Data and SpaceClaim geometry modules allow the use of imported experimental pressure data as well as the ability to quickly modify projectile geometries without leaving ANSYS.

3.2.1 Simulation Assumptions

Before any simulations are executed a number of assumptions need to be made that balance emulating real life conditions and lack of experimental data.

- The pressures sensed at the wall are approximate to those on the surface of the projectile. This must be made due to no instrumentation being on the projectile itself.

- The pressures sensed at the wall are symmetric axially about the projectile. Pressure sensors lie along a single line throughout the test section and only sense over a narrow angle.

- The velocity of the projectile changes consistently and approximately linearly with respect to distance between stations along the tube. With only 5 magnetic probes along each tube, velocity information is relatively low fidelity.

- The pressure profiles observed are sustained for a period of 10 microseconds to 1 millisecond. Given that sustained acceleration is seen, it is known that the pressures must be constant to some degree on the projectile but the extent of the consistency is unknown especially in baffled tube inserts.

- Any physical constraints placed on the projectile, required to run the simulation, have been placed far enough away from areas of interest that they do not effect structural loading

3.2.2 Simulation Setup

The simulations, static or transient, were set up following steps dictated by ANSYS in order to achieve reliable and accurate results. First the .csv file containing the pressure and distance data is loaded in to the External Data module identifying the first column as distance along the z axis and the second as pressures recorded in psi. This method of data importing limits variability to one dimension and one value associated with that dimension, which aligns well with the available experimental data. Next all projectiles used were drafted using SpaceClaim and the Computer Aided Designed (CAD) drawings of the P300 projectiles in question. Each of these modules were then linked to either the Static Structural or Transient Structural Models (Figure 3.5).

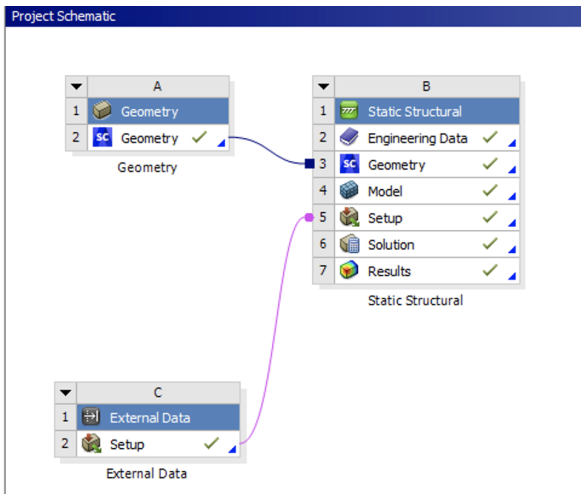

Figure 3.5: Example project schematic as viewed from the Project Page in ANSYS Workbench.

The Structural Module was then loaded using ANSYS Mechanical where projectile

components were assigned materials and meshed to appropriately small element sizes. The projectile was constrained using a surface sufficiently far away from the areas of pressure loading. In the case where the pressure loading is heavily on the rear of the projectile a small surface within the projectile at the front shoulder was specified. In the case where the pressure loading is on the shoulder or the head of the projectile the base was specified as the constraint. Structural FEA simulations require that a physical constraint be specified is order to keep the structure in question from quickly leaving the simulated conditions. In cases where allowed by the program, "inertial relief" was used which balances forces on the elements in a structural model to bring any reaction forces at the constraint to zero. This allows simulations to ignore any false stress, strain, etc. information that reaction forces may produce. Finally the External Data is imported into the simulation as a pressure load over the relevant projectile surfaces, and it is at this stage where either an analysis time is set for the Static Structural case or a simulation and load time is set for a Transient Simulation.

Having set up the simulation, it was then decided how to measure the effect of the pressure on the projectile. For this study the first of two primary measures will be the Safety Factor: the stress on each element divided by the yield stress of the material. Safety Factor is a useful tool as it allows one to easily assess the danger posed to different parts of a structure by a particular loading; as safety factor decreases towards 1 the element is approaching its yield strength and as it passes below 1 the element is now experiencing plastic deformation. The second measure in this study is a direct measure of deformation, which simply returns the distance a particular element deformed from its original position.

3.3 Polycarbonate Projectile Results

3.3.1 Consistent Performance: HS2159

The first run selected to simulate its effects was Hot Shot 2159 (HS2159). This run is meant to serve as a control to be compared to other more anomalous runs. For this run the test sections were configured as shown in Table 3.1. The change in velocity seen in this table as well as the plot of velocity versus distance in Figure 3.6 is an example of a healthy driving run in the ram stages.

Ram Stage	1 (2m)	2 (2m)
Insert Configuration	2m BTRA500	2m RTRA100
Chemistry	$1CH_4 + 2O_2 + 4.67N_2$	$2.2CH_4 + 2O_2 + 7.52N_2$
Pressure	301psi	298psi
Entrance Velocity	775 m/s	992 m/s
Δv	237 m/s	213 m/s

Table 3.1: Configuration and shot details for HS2159.

Having selected HS2159 each station's pressure profile was stepped through one by one to ensure there was no large pressure spikes or anything abnormal. Having confirmed this, the pressure profile at station 13 in ram stage 2 was selected, this pressure profile is the example shown in Figure 3.4. The pressure transposed onto the surface of a P300 polycarbonate projectile can be seen in Figure 3.7. Distinctive features to note here are the large pressure on the base and latter shoulder of the projectile which provide the large acceleration; additionally note the higher pressure bands up along the projectile shoulder which are likely results of the reflected conical shock produced by the nose traveling through 298psi gas at a speed of roughly 1075 m/s, or Mach 3.0, in this chemistry.

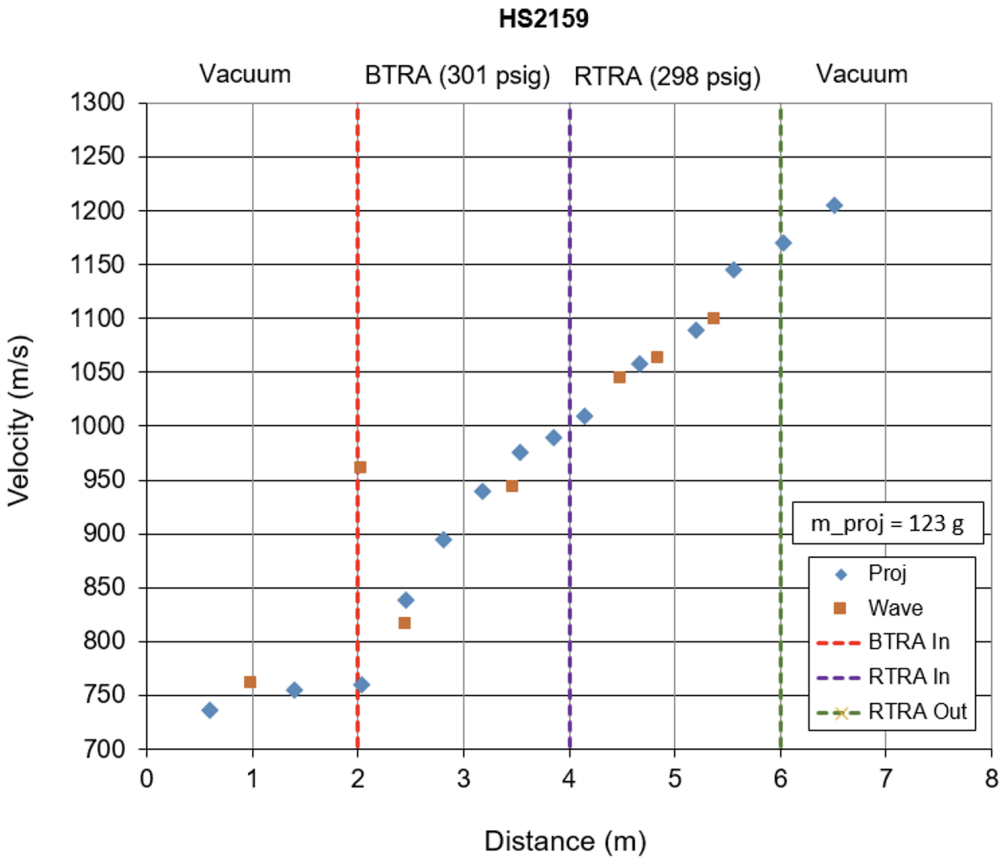

Figure 3.6: HS2159: Projectile and pressure wave velocity distribution undergoing consistent acceleration.

Before jumping into the structural analysis this pressure profile can be compared to a Computational Fluid Dynamics (CFD) simulation to verify that the pressure seen at the tube wall is a close approximation to the pressure on the projectile. Shown in Figure 3.8 is an ANSYS Fluent CFD simulation of a started ram projectile traveling through a methane-oxygen mixture at 1,400m/s. A region of high pressure on the base can be seen in both Figures 3.7 and 3.8 and slightly higher pressure region forward on the body of the projectile resulting from the reflected conical shock. This shock region is most likely further back on the simulated projectile as the Mach number is

higher resulting is a shallower shock coming off the projectile's nose. A region of high pressure spreads farther on the base of the CFD result, which may be a result of the wall pressure not exactly matching the projectiles surface in the experimental study. Despite some variation the trends of the pressure profiles are close enough that the structural simulation using experimental data still has value.

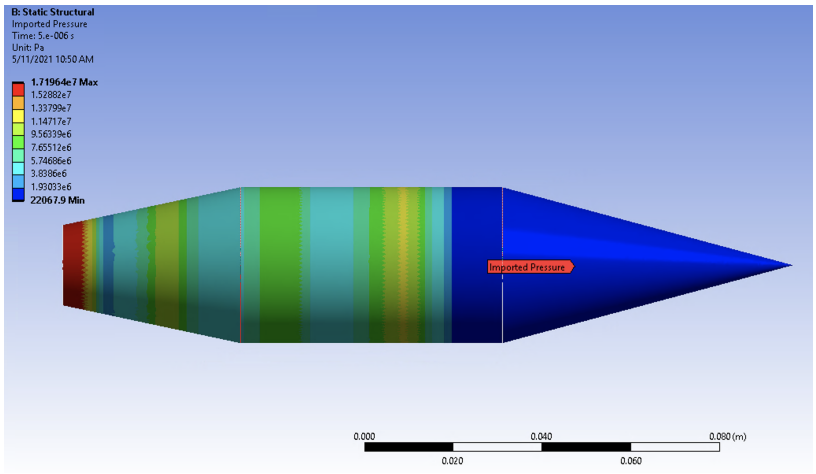

Figure 3.7: Steady driving pressure overlaid on a P300 polycarbonate projectile.

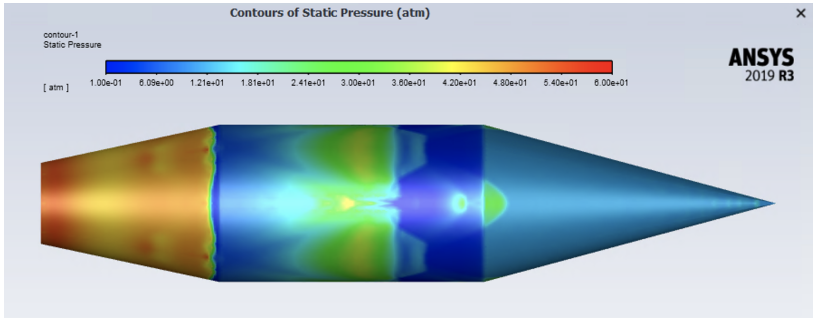

Figure 3.8: CFD Simulation: Gas and rail inserts travelling at 1,400m/s at inlet towards stationary projectile. Chemistry is $1.8CH_4+2O_2+7.52N_2$ at 75psi. Simulated by Navid Daneshvaran using ANSYS Fluent.

Running this pressure in an ANSYS Static Structural module was a low computational load and quickly delivered the results of interest: safety factor and deformation, and to little surprise the projectile easily endured this pressure load. The safety factor showed a minimum value of 3.64 at the edges where the polycarbonate projectile interacts with the nylon plug which is also of little surprise given the relatively soft nylon being used. And exterior view as well as a section view of the safety factor can be seen in Figures 3.9 and 3.10 respectively.

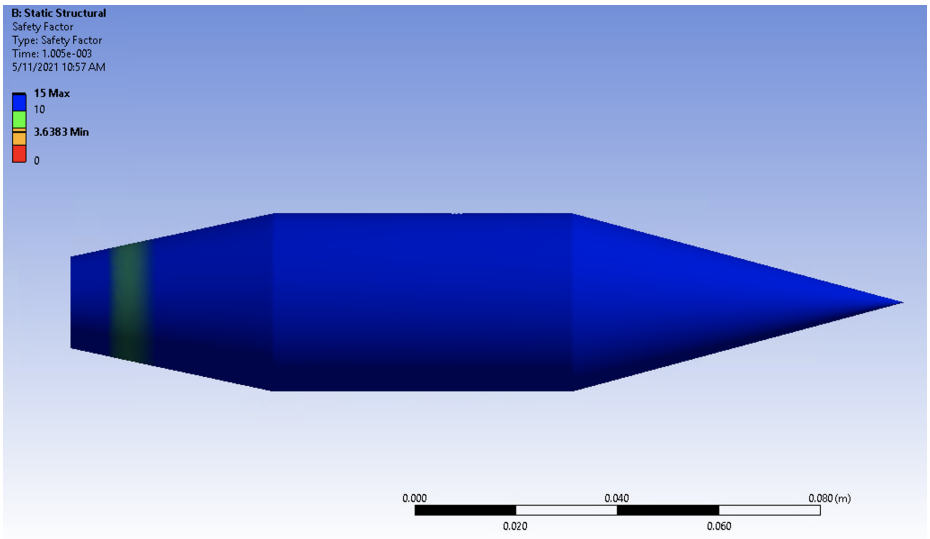

Figure 3.9: Safety factor resulting from steady driving acceleration on P300 polycarbonate projectile.

The deformation to the projectile due to the pressure loading was minimal with a maximum deformation of 0.125mm on parts of the projectile base, a number that is still very firmly elastic deformation. The surface deformation and section view of deformation can be seen in Figures 3.11 and 3.12 respectively. Having examined both the safety factor and deformation resulting from the pressures seen in HS2159 it can be concluded that the projectile's structural integrity is not being compromised under these conditions and will serve as an adequate control case.

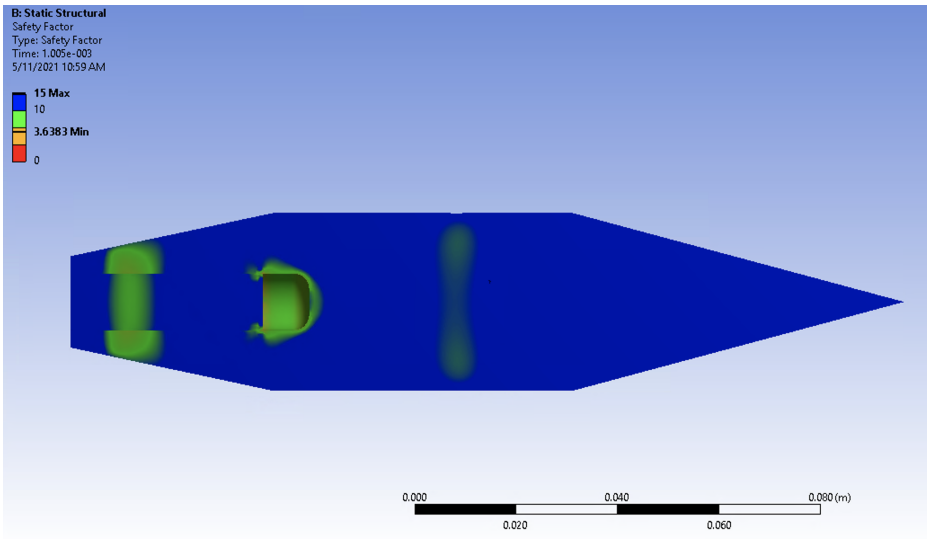

Figure 3.10: Sectioned view showing safety factor resulting from steady driving acceleration on P300 polycarbonate projectile.

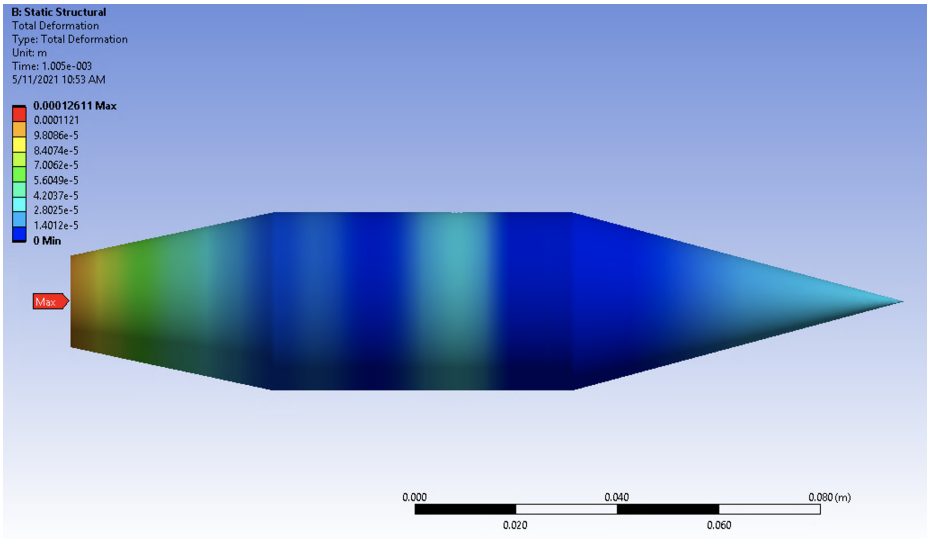

Figure 3.11: Deformation resulting from steady driving acceleration on P300 polycarbonate projectile.

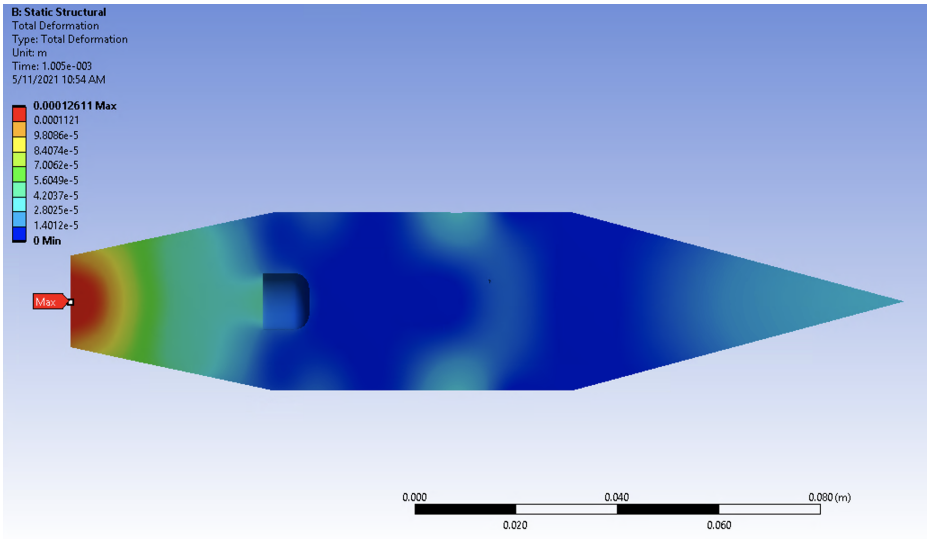

Figure 3.12: Section view of deformation resulting from steady driving acceleration on P300 polycarbonate projectile.

3.3.2 Unexplained Drop in Performance: HS2168

The run selected to compare to HS2159 where an unexplained drop in performance is seen is Hot Shot 2168 (HS2168). This run was configured similarly to HS2159 in that the chemistry in each tube as well as the insert configurations were identical. The only changes made were to fill pressure and entrance velocity. The configuration of the ram stages and velocities can be seen in Table 3.2. These changes were made incrementally in a series of experiments where Mach limits of the rail and baffle inserts were being explored. By increasing the fill pressure, the change in velocity for each section was expected to increase in order to probe higher Mach numbers; however, there was an unexpected large decrease in performance in ram stage 2 following increasingly large pressure spikes at stations 10 and the insert in ram stage 1. The decrease in performance can also be seen in the plot of the velocities of the projectile and pressure wave in Figure 3.13. Note that these distribution are "messy" compared to those in Figure 3.6. This increased level of noise often accompanies larger pressure spikes, but the lower Δv is clear and present regardless.

Ram Stage	1 (2m)	2 (2m)
Insert Configuration	2m BTRA500	2m RTRA100
Chemistry	$1CH_4 + 2O_2 + 4.67N_2$	$2.2CH_4 + 2O_2 + 7.52N_2$
Pressure	450psi	350psi
Entrance Velocity	1031 m/s	1270 m/s
Δv	239 m/s	96 m/s

Table 3.2: Configuration and shot details for HS2168.

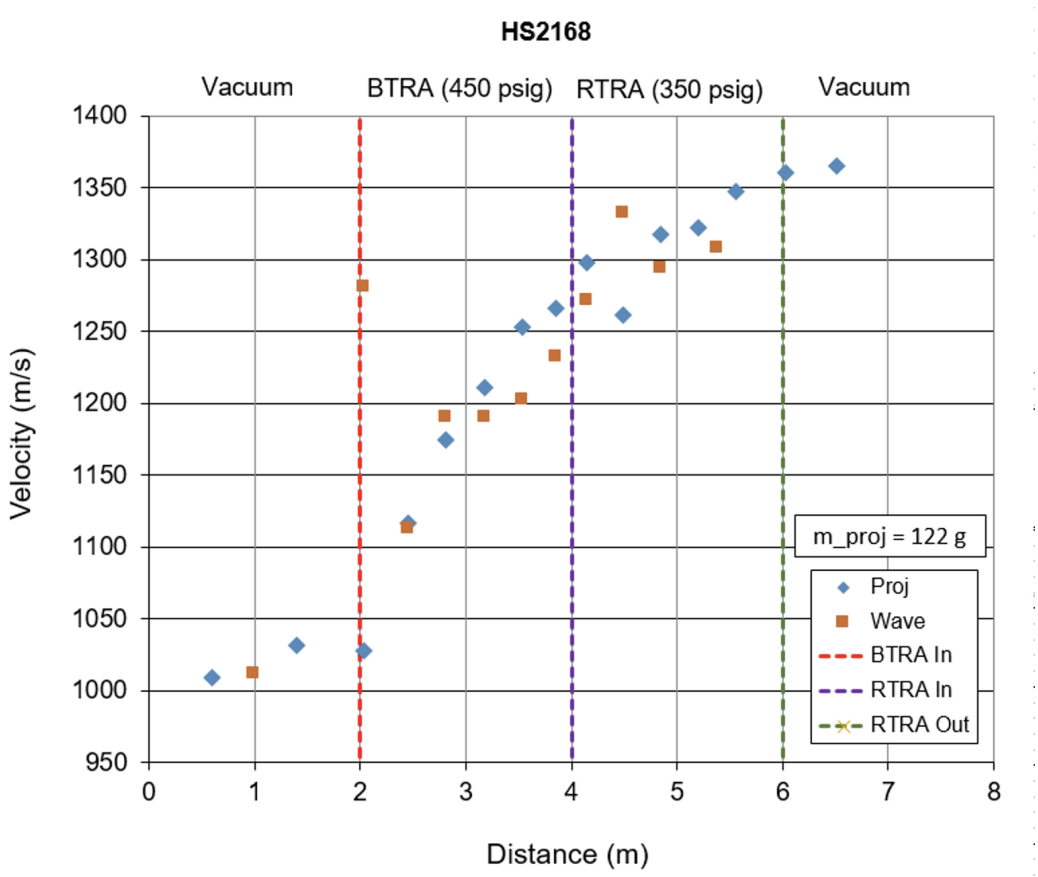

Figure 3.13: HS2168: Projectile and pressure wave velocity distribution with an unexplained drop in performance in the RTRA Section.

The high pressure spikes in question can be seen in Figure 3.14 have magnitudes up to nearly 40,000psi seen at the insert pressure probe. Upon closer inspection it can be seen that the spikes do not lie just behind the projectile, as peak combustion pressures often do, but they are actually up on the mid tail and the body of the projectile. These large pressures being on the polycarbonate body is evidence that something structurally may have happened to the projectile to generate the decrease in performance; therefore, the effects of these pressures must be explored to determine if this is the case.

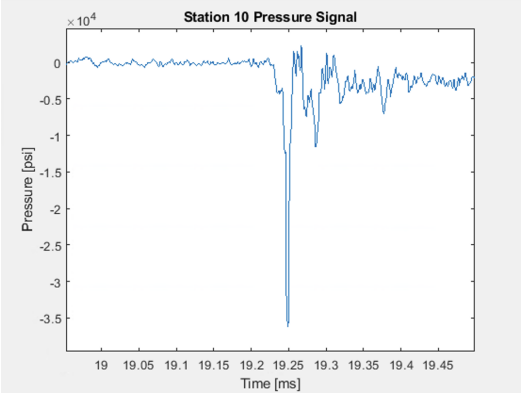

(a) Pressure signal at station 13. Note the spike in pressure to 35ksi.

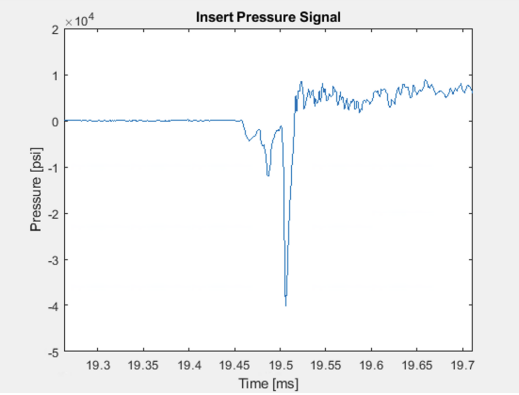

(b) Pressure signal at station 13. Note the spike in pressure to 40ksi.

Figure 3.14: Unusually high pressure signals from the end of the BTRA section, just before reduced performance.

The first pressure to be simulated is station 10 shown in Figure 3.14(a). By overlaying this profile over a P300 polycarbonate projectile (Figure 3.15) a large band of extremely high pressure just behind the middle of the projectile can be seen. This is indicative of the onset of an unstart, likely due to the velocity and chemistry mixture resulting in too much heat release and the combustion beginning to overtake the projectile. No unstart was seen during this run which means the baffles were successfully delaying a full unstart. Considering projectiles may enter the state of nearly unstarting and continue to drive in the future, it is important to determine the effects on the projectiles structure.

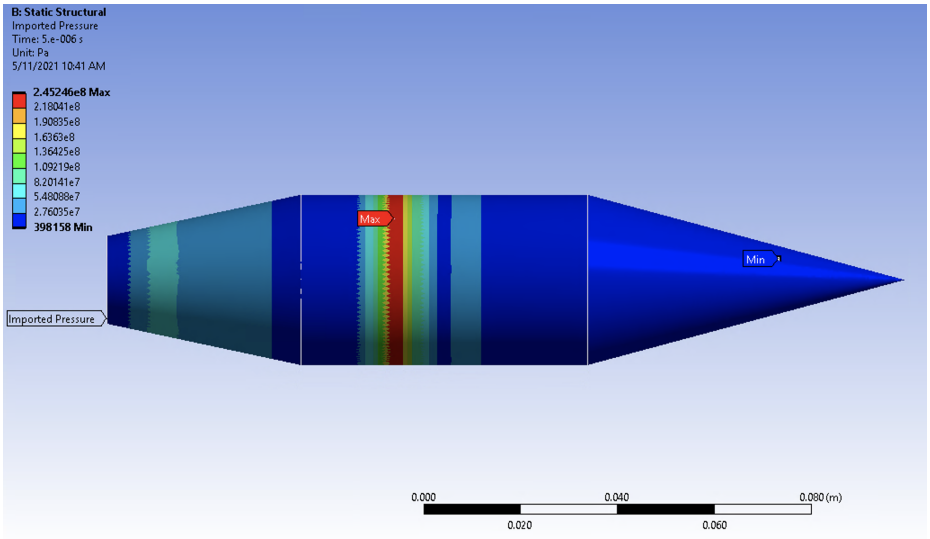

Figure 3.15: P10 High pressure spike overlaid on a P300 polycarbonate projectile.

Figure 3.16 shows the safety factor on the surface of the projectile; it can be seen that an appreciable amount of the surface has a safety factor below 1 indicating that the surfaces are yielding at the high pressure location and in the area around it. Examining the section view of the safety factor shown in Figure 3.17 shows that the region containing a safety factor below 1 reaches all the through the projectile indicating yielding throughout.

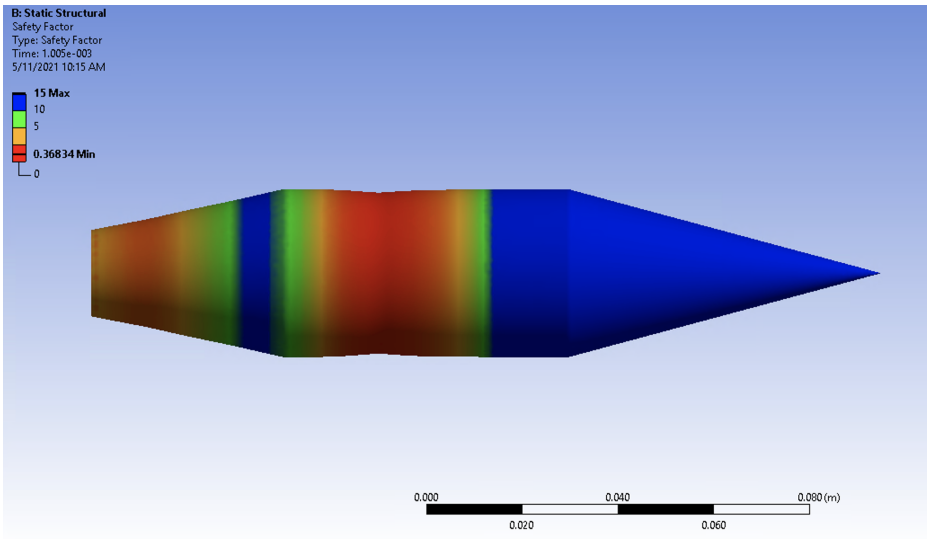

Figure 3.16: Safety factor resulting from P10 high pressure spike on P300 polycarbonate projectile.

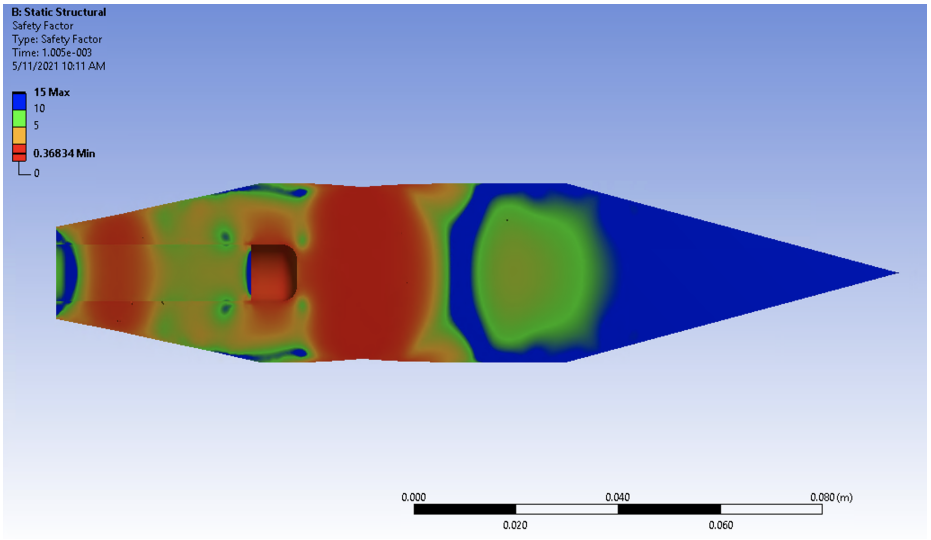

Figure 3.17: Section view of safety factor resulting from P10 high pressure spike on P300 polycarbonate projectile.

The pressures detected at station 10 are causing a large amount of yielding throughout the projectile body. Looking then at the deformation, Figures 3.18 and 3.19 show that at the maximum the body is deforming 0.8mm, which may seem low but compared to the radius of the projectile this value is around 5% of the total distance it can be deformed. Large deformations are occurring and it must be asked if a Static Structural simulation is appropriate or are the times over which these pressures are being applied too short to actually propagate the stresses and cause this amount of damage. Therefore a transient structural simulation must be performed in order to corroborate the results shown in the static simulation.

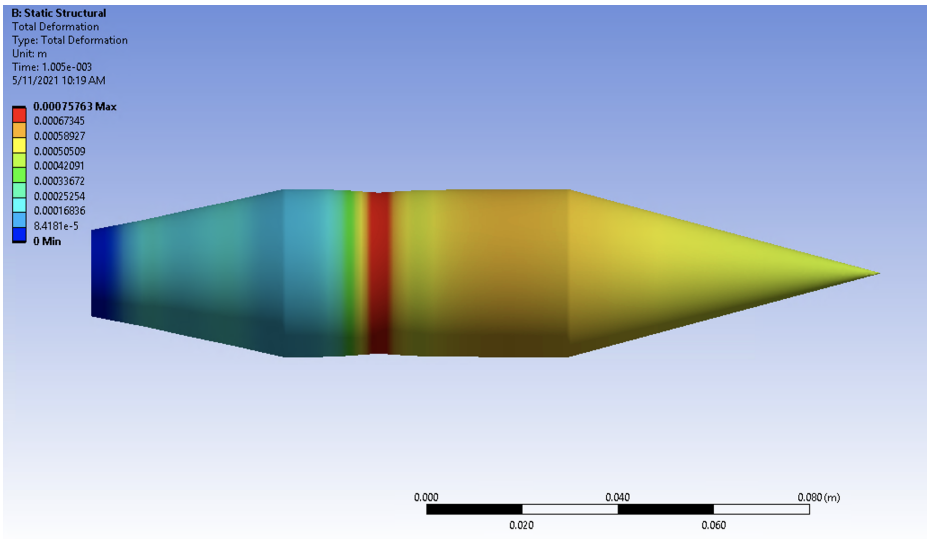

Figure 3.18: Deformation resulting from P10 high pressure spike on P300 polycarbonate projectile.

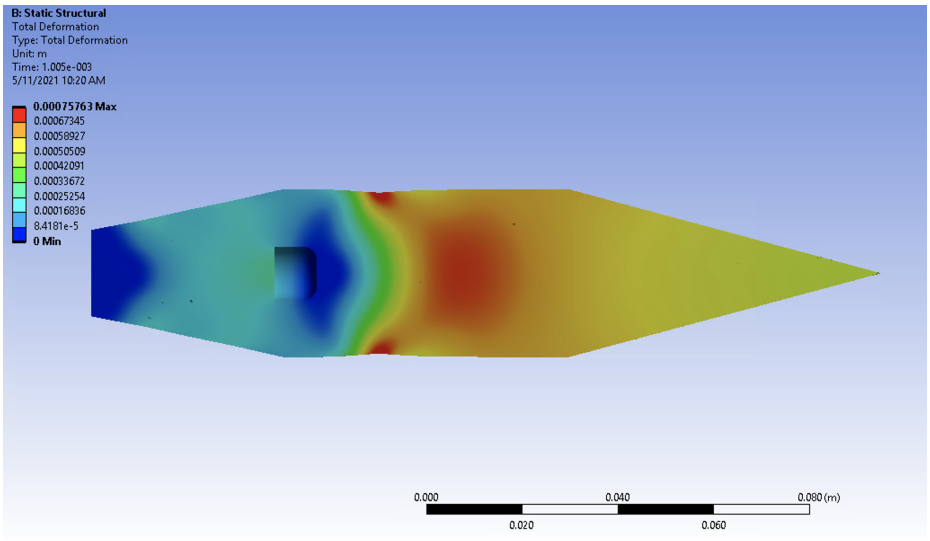

Figure 3.19: Section view of deformation resulting from P10 high pressure spike on P300 polycarbonate projectile.

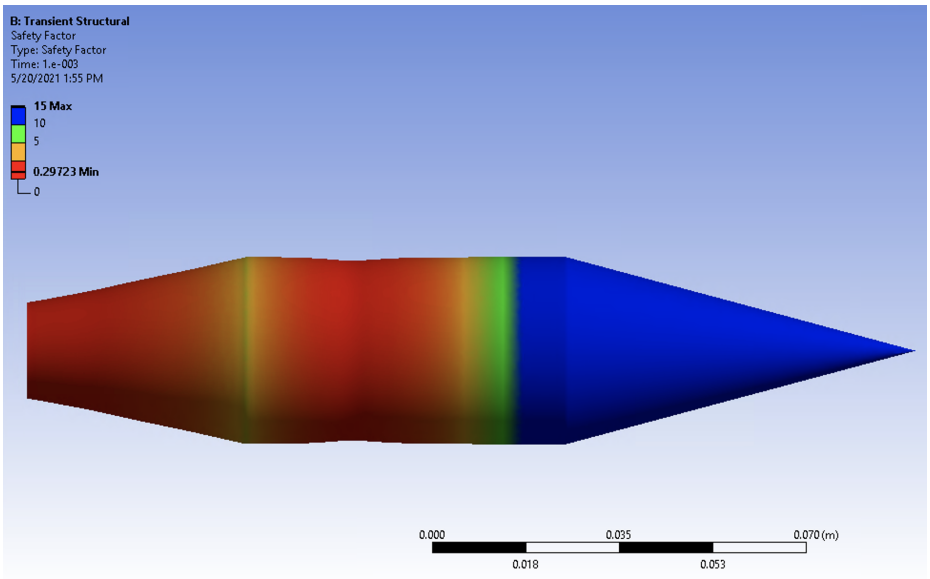

Figure 3.20: Transient Simulation. Safety factor resulting from P10 high pressure spike on P300 polycarbonate projectile.

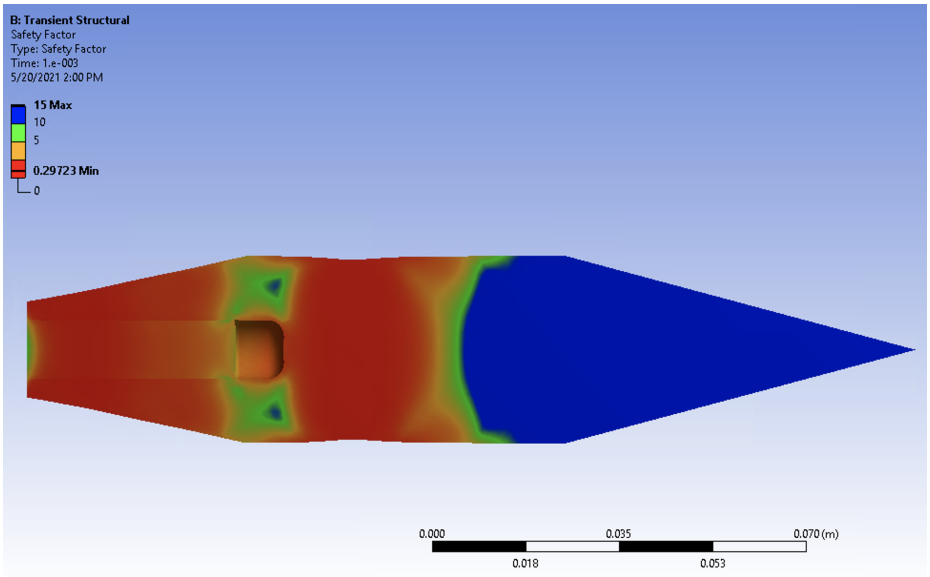

Figure 3.21: Transient Simulation. Section view of safety factor resulting from P10 high pressure spike on P300 polycarbonate projectile.

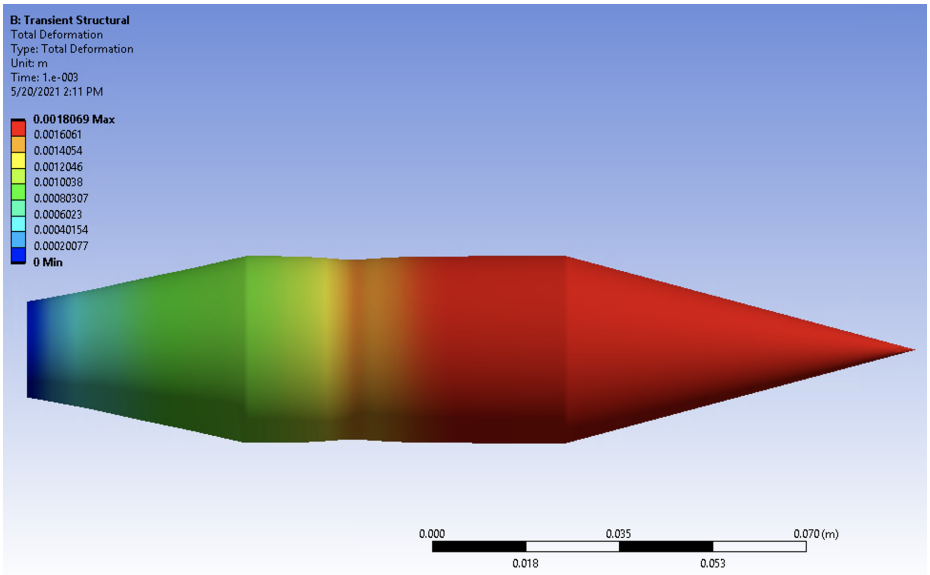

Figure 3.22: Transient Simulation. Deformation resulting from P10 high pressure spike on P300 polycarbonate projectile.

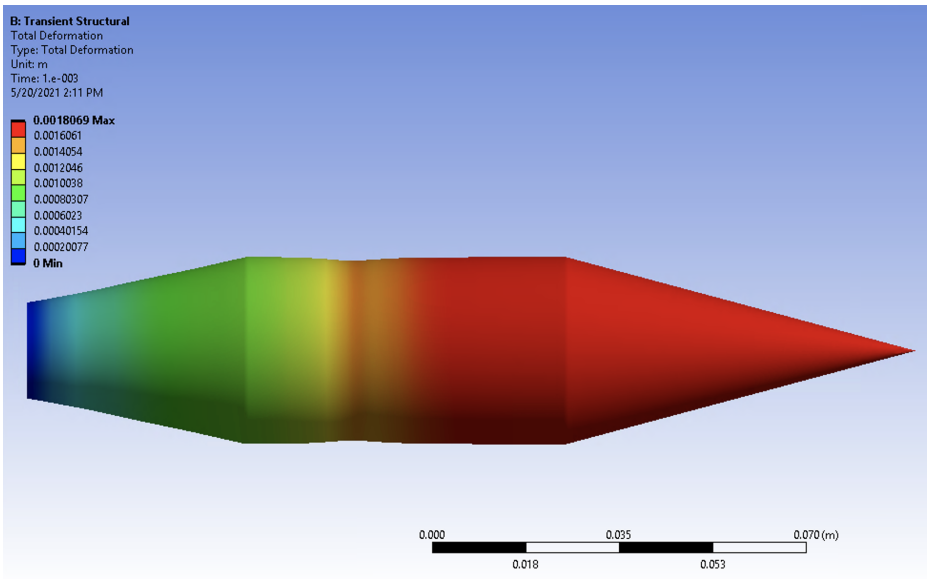

Figure 3.23: Transient Simulation. Section view of deformation resulting from P10 high pressure spike on P300 polycarbonate projectile.

Figures 3.20, 3.21, 3.22, and 3.23 show the safety factors and the deformations resulting from the pressures at station 10 when ran through a transient simulation. The magnitudes of safety factor and deformation vary slightly between the transient simulations and static simulations whenever the safety factor drops below 1 or the deformation reaches beyond elastic; however, they match within a small variance when in the elastic region and therefore it can be concluded that the static simulations adequately demonstrate the physical effects of these pressures for the sake of this study. Moving forward only static simulations were performed as a means to save on computation hours as the transient studies took around 2 orders of magnitude longer to run when compared to the static studies. It is likely that the static studies approximate the transient ones well due to the high speed of sound in polycarbonate. Force and displacement information can propagate through the material faster than changes in the loading on the projectile; the timescales of deformation for the projectile are small enough that transient effects are minimal in this study.

Having established the use of static structural studies being adequate, the next pressure spike was explored. Following the station 10 large spike in pressure on the body of the projectile, an even larger spike was seen at the insert between the 2 ram stages. The pressure profile reaching up to almost 40,000psi is shown in Figure 3.14 (b). Overlaying the pressure onto the projectile (Figure 3.24) shows that the pressure spike is now further back on the tail of the projectile. The high combustion pressures on the projectile being pushed back is evidence that the baffled tubed inserts are performing well at "pushing" back unstarts as they try to occur which corroborates the results shown in previous studies [8].

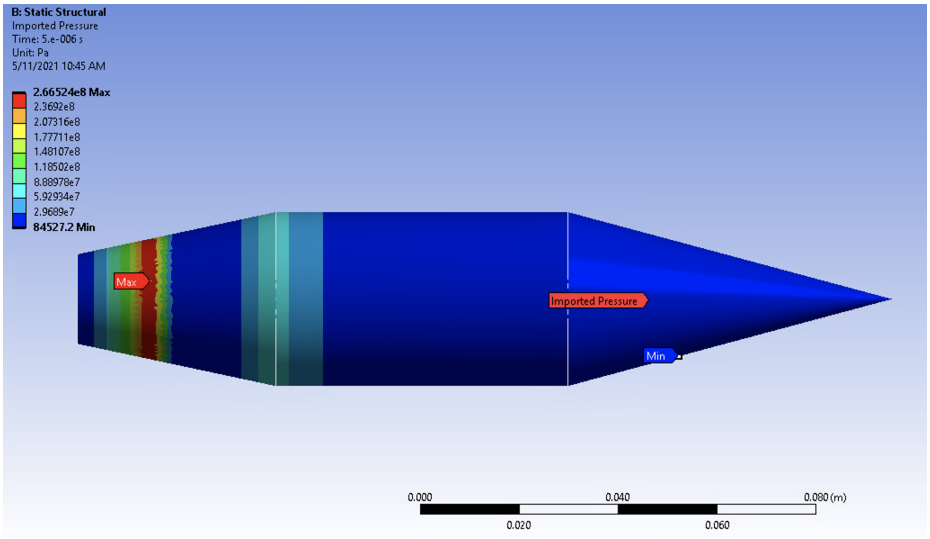

Figure 3.24: Ptrin High pressure spike overlaid on a P300 polycarbonate projectile.

Simulations of the insert pressure on the projectile were slightly more intensive due to the presence of the pressure spike being directly over the projectiles nylon plugged bore hole. The open space in this structure allows greater leeway for deformation and less support to resist it. This is shown in the Figures 3.25 and 3.26 where the lowest values of safety factor are beneath the pressure spike and along the surface of the bore hole. A large region exists where the safety factor drops below 1 indicating a failure in structural integrity. Interestingly this large pressure spike would accelerate the projectile much more than the lower driving pressures seen earlier; however the large amount of plastic deformation done to the structure shown in Figures 3.27 and 3.28 is clearly compromising the integrity of the polycarbonate projectile.

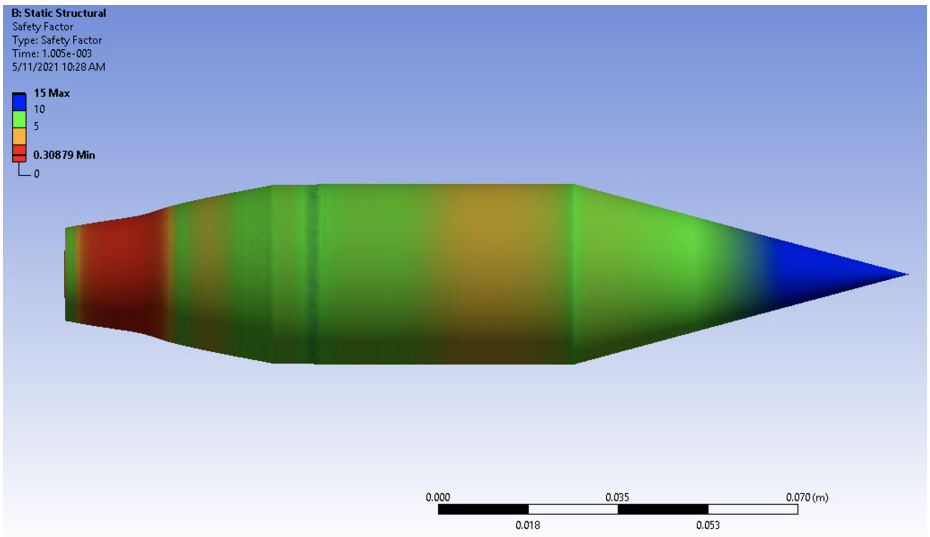

Figure 3.25: Safety factor resulting from Ptrin high pressure spike on P300 polycarbonate projectile.

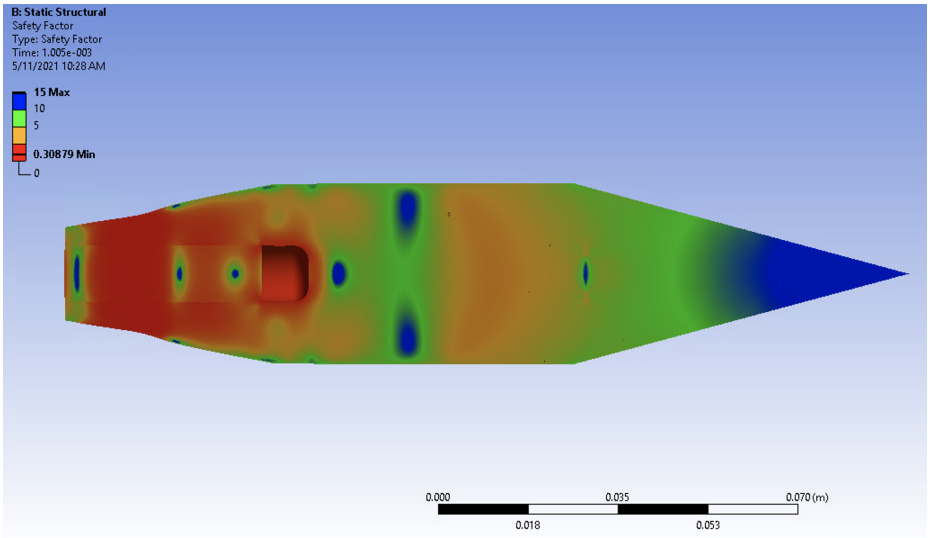

Figure 3.26: Section view of safety factor resulting from Ptrin high pressure spike on P300 polycarbonate projectile.

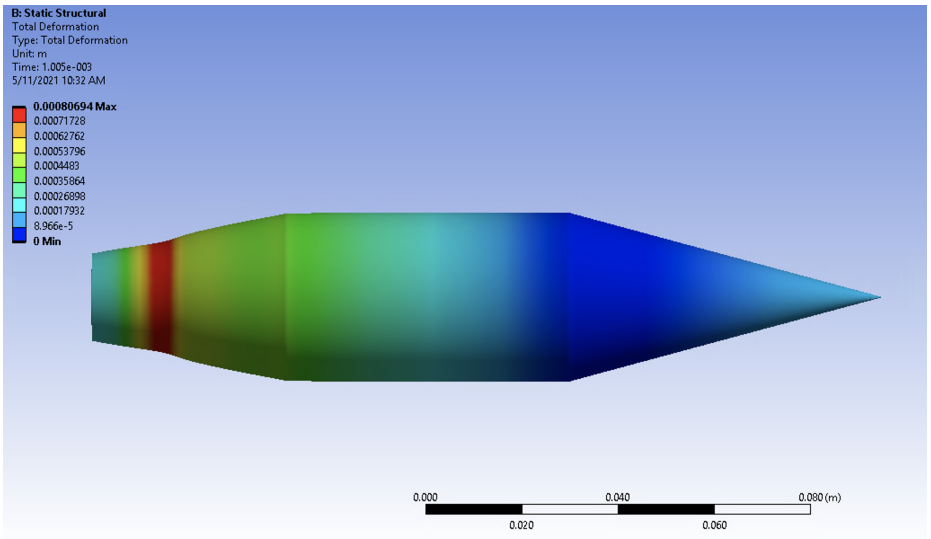

Figure 3.27: Deformation resulting from Ptrin high pressure spike on P300 polycarbonate projectile.

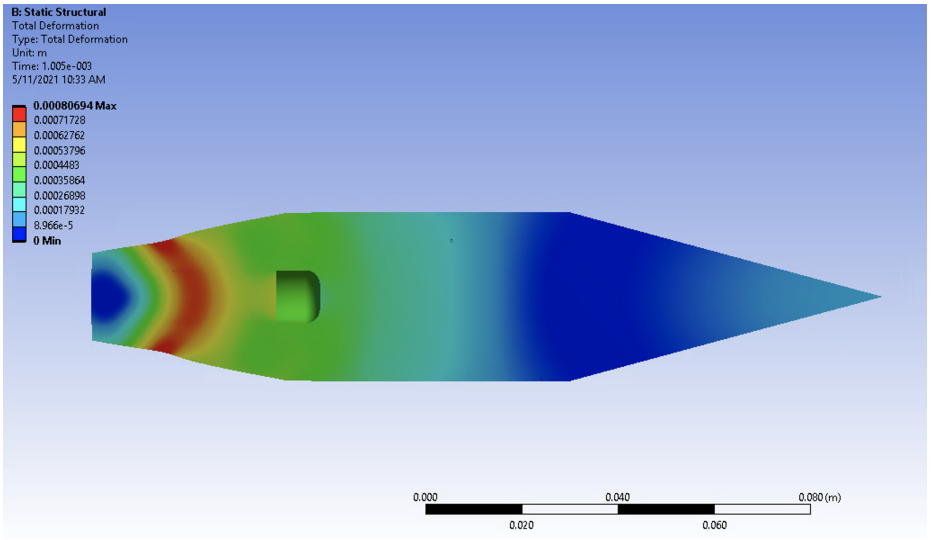

Figure 3.28: Section view of deformation resulting from Ptrin high pressure spike on P300 polycarbonate projectile.

3.3.3 Deformation Effects on Flow Field

It has been demonstrated that deformation occurs both on the body of the projectile as well as on the projectile tail as a result of the pressures obtained during experimentation. The modified surfaces of the projectile likely lead to increased levels of drag resulting in a drop in performance, as seen during experimentation. This effect can be explained by approximating the resultant deformation as a wave shaped wall along the projectile's surface and analyzing the effects on the flow.

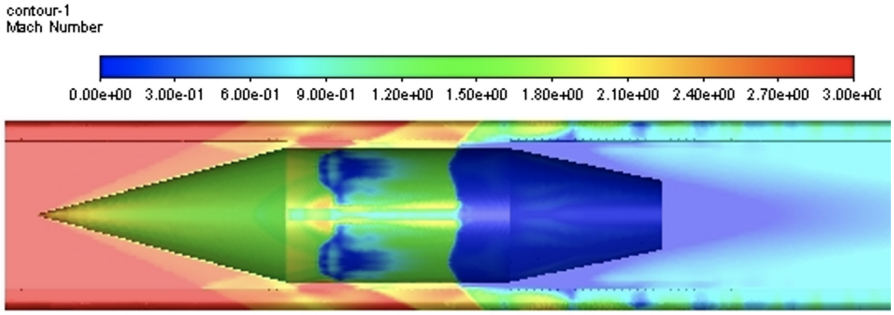

Figure 3.29: CFD Simulation: Gas and rail inserts travelling at 1,200m/s at inlet towards stationary projectile. Chemistry is $1.8CH_4+2O_2+7.52N_2$ at 75psi. Simulated by Navid Daneshvaran using ANSYS Fluent.

CFD simulations (Figure 3.29) indicate that the flow around the deformed area on the body of the projectile during normal operation in railed tube are between Mach 1.5 and Mach 2. Supersonic flow passed a wave shaped wall results in a sinusoidal pressure distribution where the maximum pressure lies on the "front facing" side of the trough-like deformation and the minimum lies on the "back facing" side of the deformation [19]. During the time where the pressure spike is present on the projectile's body, the increased pressure from the flow likely generates a greater amount of yielding which would widen the deformation until the large pressure spike is "pushed back" by the baffle geometry. Additionally this difference in pressure across the deformation will

lead to production of drag on the projectile, resulting in a performance drop that is proportional to the depth of the deformation.

Conversely, CFD simulations (Figure 3.29) indicate that the flow around the deformed region on the tail of the projectile is subsonic, between near Mach 0 and Mach 0.8. Subsonic flow passed a wave shaped wall also results in a sinusoidal pressure distribution; however, it is in phase with the wave-like shape of the wall [19]. The maximum pressure lies at the bottom of the deformed trough and the minimum lies at the peak. This results in no net drag on the projectile, but the increased pressure added to the pressure spike on the yielded region will likely lead to greater deformation. As these pressures are proportional to the depth of the deformed region it is likely this process would form a loop of deepening plastic deformation and increasing pressure until the baffles "push back" the region of high pressure.

Although the approximation of a wave like wall gives some incite into the effects of the deformed surfaces on the flow and how those effects may result in drag, it is still an approximation. To better understand what is occurring, CFD simulations would need to be pursued where a deformed projectile is simulated such as in Figure 3.29.

3.4 Aluminum Projectile Results

Having simulated the consequence of steady driving pressures and high pressure spikes on a polycarbonate projectile and seeing clear signs of structural integrity being compromised, the first natural step is the move to a stronger lightweight material: aluminum. The ram lab has used several different variations of the P300 projectile made of 6061 aluminum, and is currently using P300AL projectiles for some of the high pressure experiments. An aluminum projectile was run through the same simulations as the polycarbonate projectile discussed in the previous section in order to see if it resists deformation in the face of the high pressure spikes. It is important to note that the aluminum projectiles were not used for HS2159 and HS2168, and this simulation is being done as a comparison rather than to examine what occurred on those runs.

3.4.1 Consistent Performance: HS2159

The pressure profile from station 13 of run HS2159 was laid over the projectile just as with the polycarbonate projectile in Figure 3.7 and the simulation was run under identical conditions with 6061 aluminum instead of polycarbonate. The resulting safety factor and deformations (Figures 3.30, 3.31, 3.32, 3.33) show the the projectile relatively unfazed by the pressure on the base with a lowest safety factor of 3.48 and little elastic deformation. The only real deformation seen on the projectile is the nylon plug used to hold in the magnet.

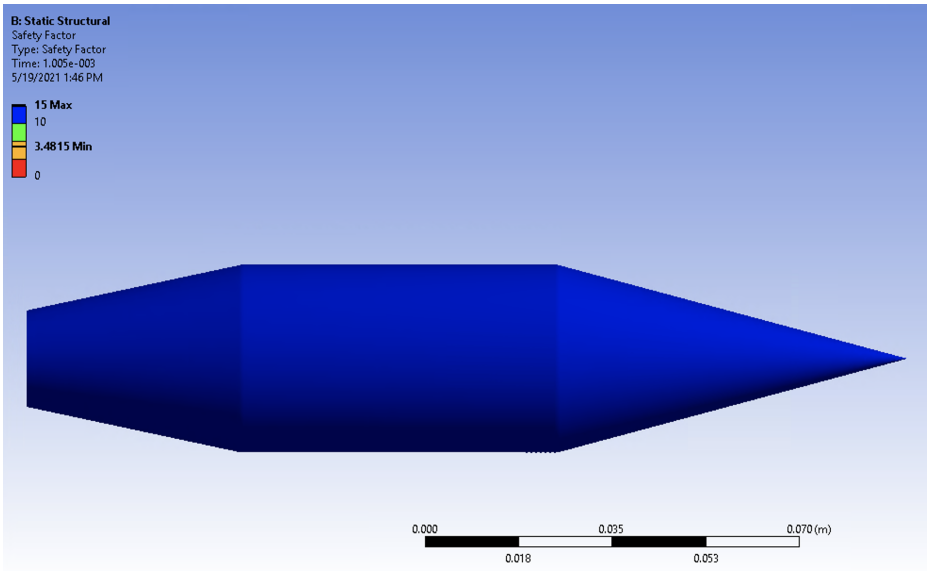

Figure 3.30: Safety factor resulting from steady driving acceleration on P300 aluminum projectile.

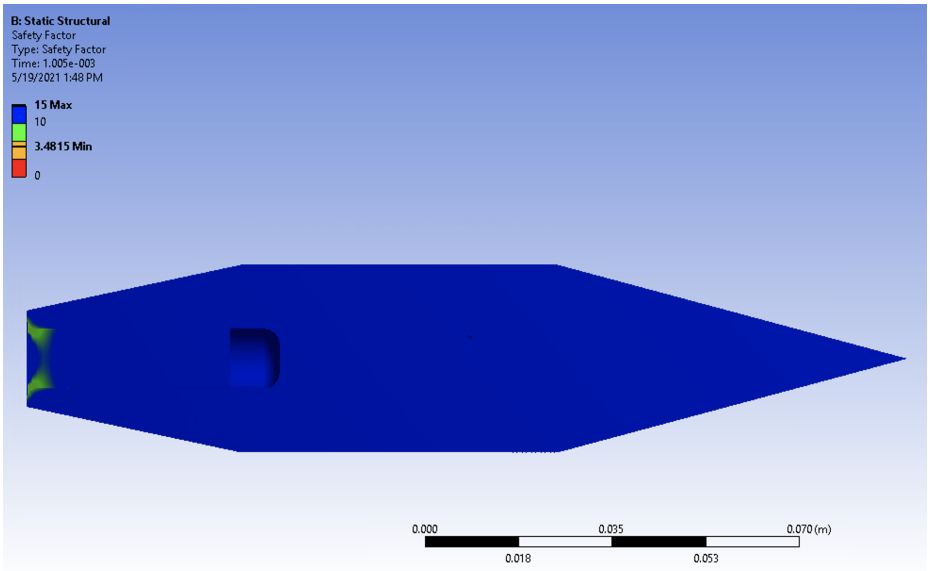

Figure 3.31: Section view of safety factor resulting from steady driving acceleration on P300 aluminum projectile.

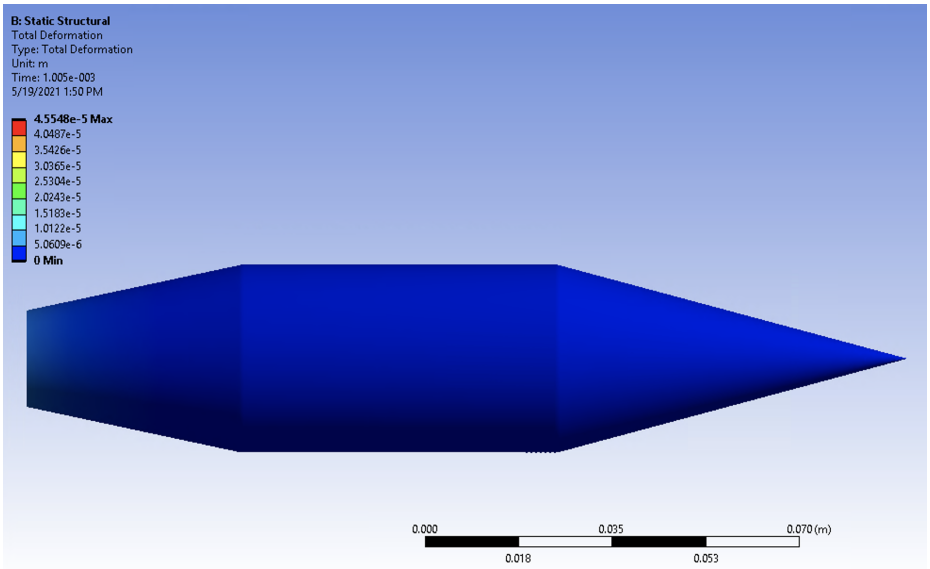

Figure 3.32: Deformation resulting from steady driving acceleration on P300 aluminum projectile.

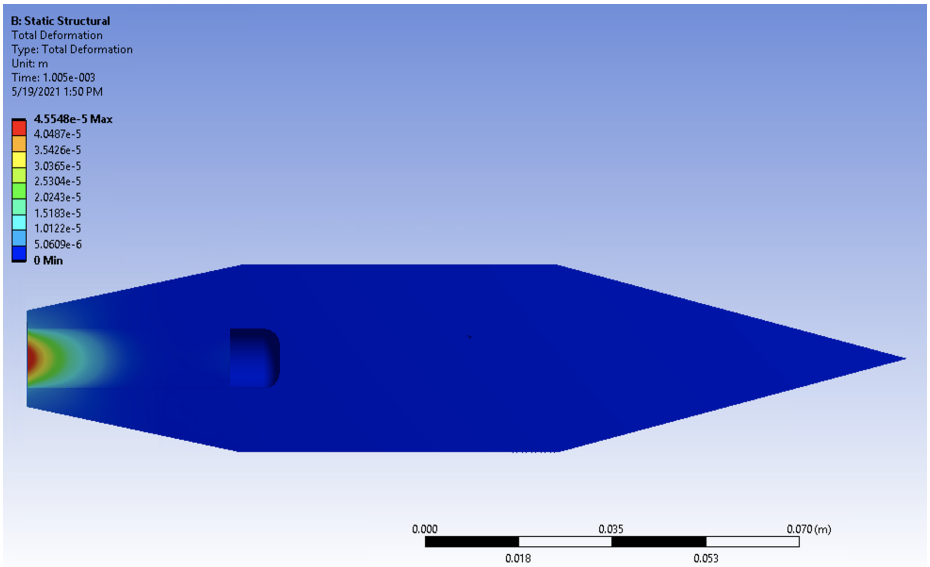

Figure 3.33: Section view of deformation resulting from steady driving acceleration on P300 aluminum projectile.

3.4.2 Unexplained Drop in Performance: HS2168

Having demonstrated the robustness of the aluminum projectile during nominal operation, the projectile integrity was then assessed with the large pressure spikes seen at station 10 and the insert. The pressure at station 10 was first considered and laid over the projectile just as in Figure 3.15.

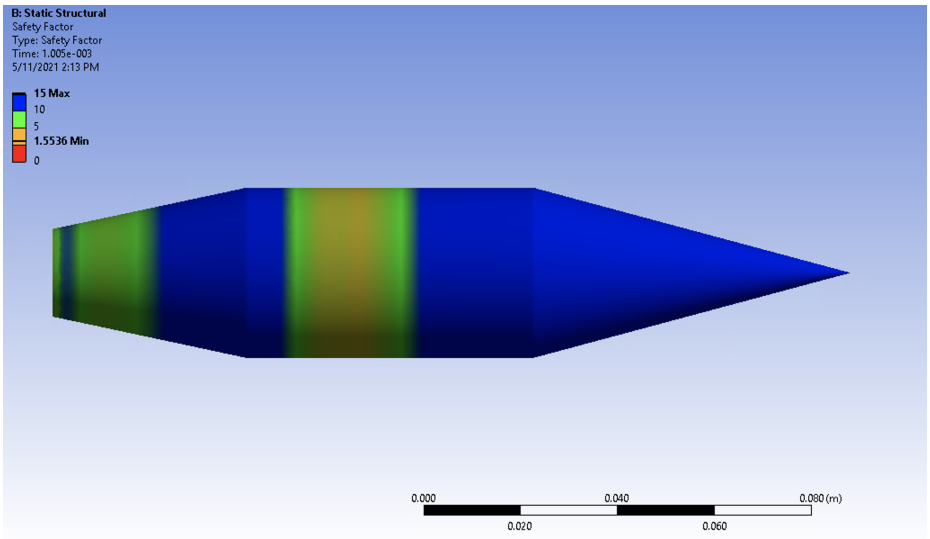

Figure 3.34: Safety factor resulting from P10 high pressure spike on P300 Aluminum projectile.

It can be seen from the exterior and section views of the safety factor shown in Figures 3.34 and 3.35 that the value of safety factor does not drop below 1.55. While this value is lower than what a part is safely designed to, it shows that at no point in the projectiles body is yielding occurring as a result of the high pressure spike along its body. This is corroborated by Figures 3.36 and 3.37 that show a small amount of elastic deformation.

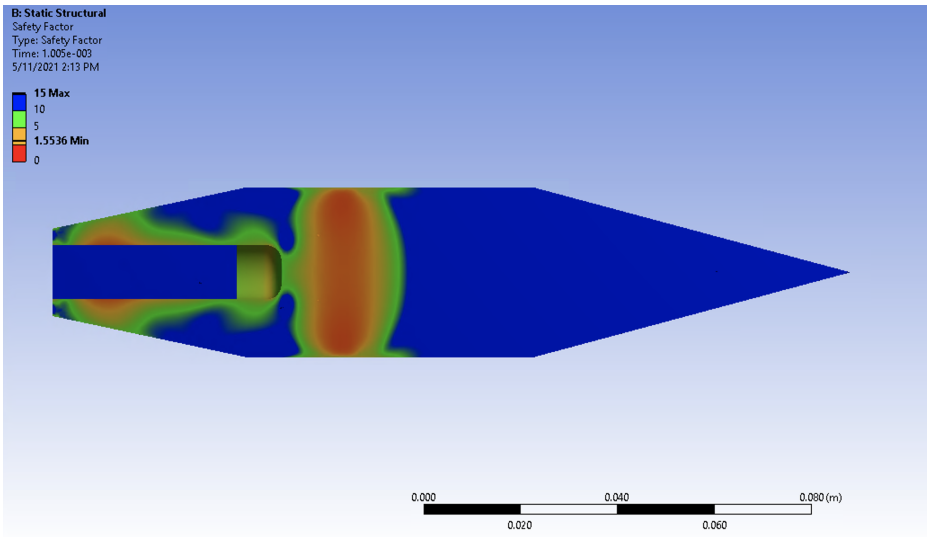

Figure 3.35: Section view of safety factor resulting from P10 high pressure spike on P300 Aluminum projectile.

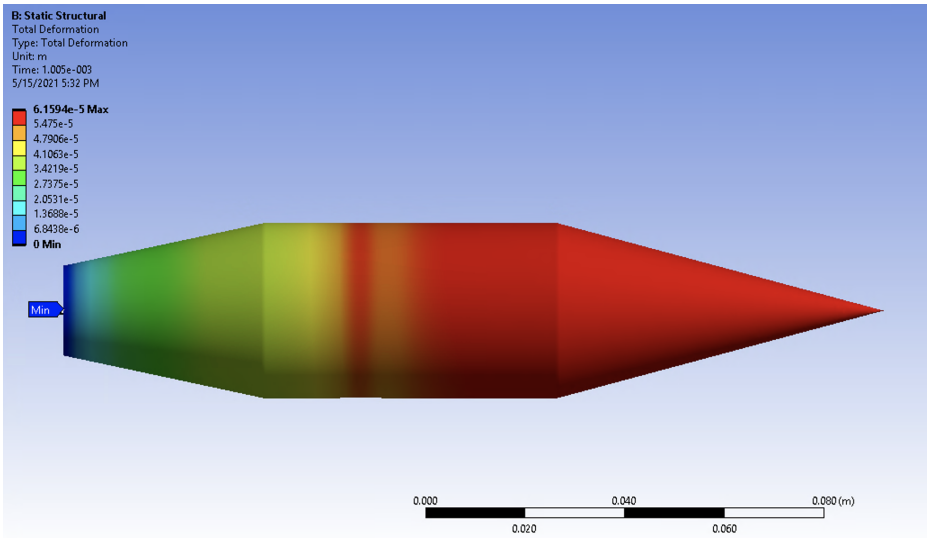

Figure 3.36: Deformation resulting from P10 high pressure spike on P300 Aluminum projectile.

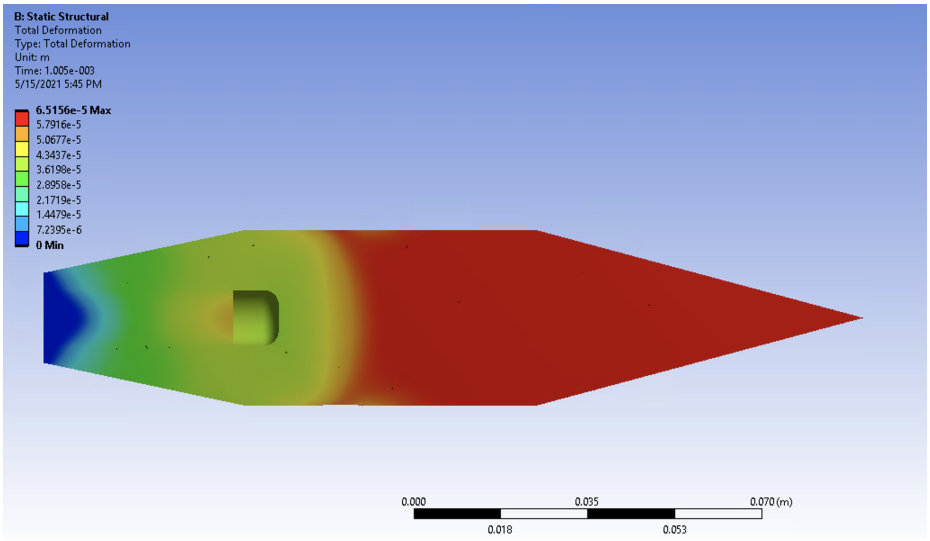

Figure 3.37: Section view of deformation resulting from P10 high pressure spike on P300 Aluminum projectile.

Having seen low, but over 1, safety factors and some elastic deformation of the aluminum P300 projectile loaded with the pressure signal from station 10, the insert signal was then examined. In this case, the insert signal is of greater concern as it is loaded over the more complex rear geometry of the projectile which is structurally weakened by the bore hole through the base. Just as before, the pressure signal from the insert was laid over the projectile (Figure 3.24).

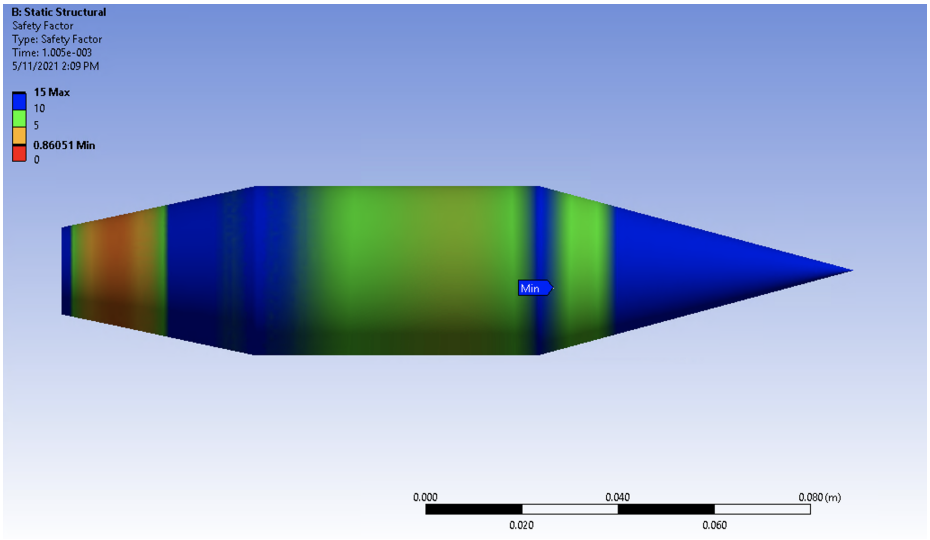

Figure 3.38: Safety factor resulting from Ptrin high pressure spike on P300 Aluminum projectile.

Figures 3.38 and 3.39 show the safety factor for the Ptrin pressure signal drops lower than for the P10 signal. Directly beneath the spike in pressure the saftey factor internally drops close to 1 but never below it. The only place the safety factor drops below 1 is the front of the projectile where it is being constrained; therefore, these are fictitious stresses and should not be regarded as experimentally relevant. Again, looking at the deformation: elastic deformation exists especially beneath the pressure spike but at no point does the solid aluminum P300 projectile experience plastic deformation.

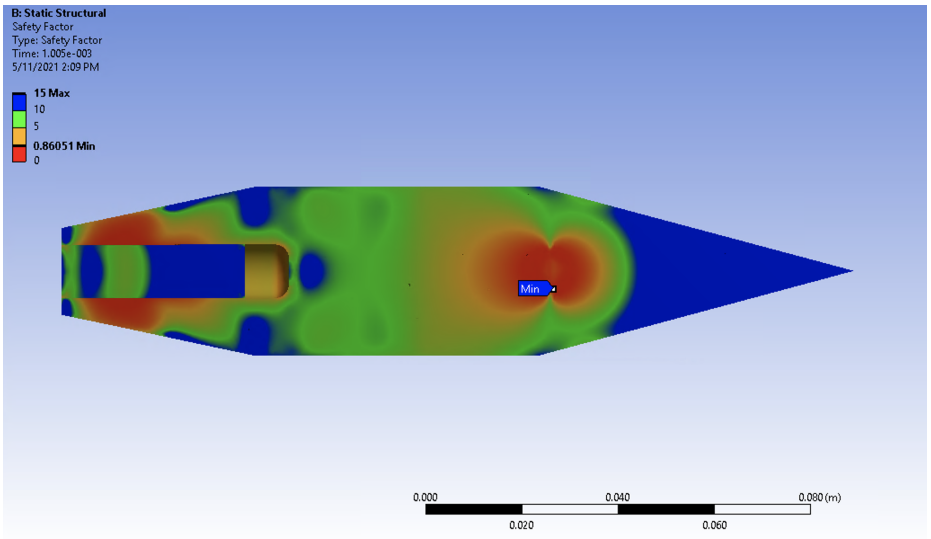

Figure 3.39: Section view of safety factor resulting from Ptrin high pressure spike on P300 Aluminum projectile.

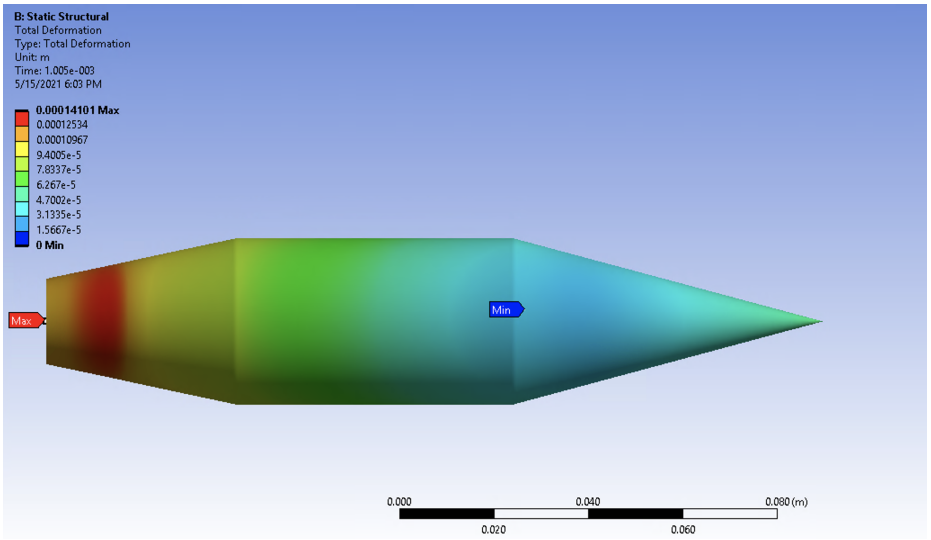

Figure 3.40: Deformation resulting from Ptrin high pressure spike on P300 Aluminum projectile.

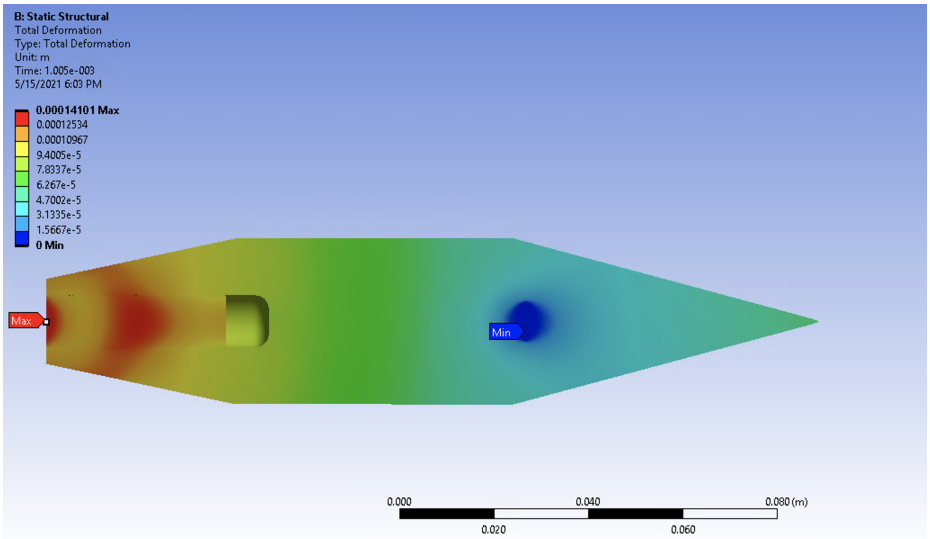

Figure 3.41: Section view of deformation resulting from Ptrin high pressure spike on P300 Aluminum projectile.

3.5 Shelled Projectile Results

The polycarbonate P300 projectile has been show to deform under the higher pressure spikes from HS2168; additionally the solid aluminum P300 projectiles have been shown to endure the same high pressure spikes without experiencing plastic deformation. Naturally, aluminum projectiles should then be used exclusively in experimentation going forward to ensure projectile integrity; however, the currently helium light gas gun can not launch the aluminum projectiles beyond 800m/s fundamentally limiting the velocity/Mach regions that can be explored. In order to launch projectiles to 1000m/s the combined weight of the obturator and projectile must be below 180g. The shelled projectile design discussed earlier was developed for just this case: to maximize structural integrity while minimizing the weight. The shell aluminum P300 was tested in the control HS2159 case where there was steady driving acceleration and the deformation results and safety factor show the expected extremely high safety factors and minimal elastic deformation. The Figures are attached in Appendix A for completeness (Figures A.2, A.3, A.4, A.5).

3.5.1 Unexplained Drop in Performance: HS2168

The shelled projectile was first tested with the pressure profile from Station 10 during HS2168 just as with the polycarbonate and the aluminum projectiles. The pressure was laid over the projectile (Figure 3.15) and a structural simulation was run.

An initial look at Figures 3.42 and 3.43 show that the safety factor drops lower than that of the solid aluminum projectile; however, it only drops below 1 on the interior wall of the rear part of the projectile. The exterior of the projectile maintains a safety factor over 1.5. Despite the drop in safety factor on the interior it can be seen from Figures 3.44 and 3.45 that the deformation is minimal and still well within what is considered elastic.

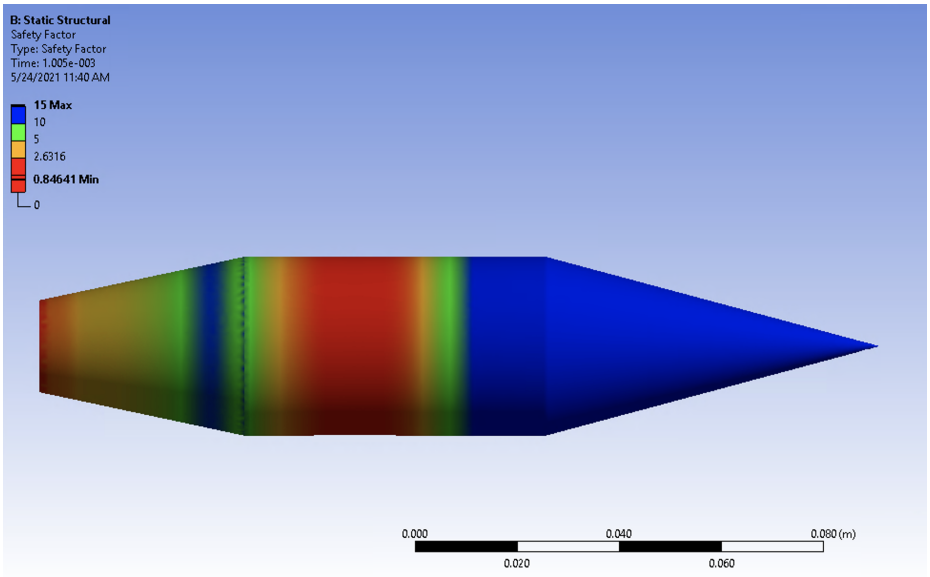

Figure 3.42: Safety factor resulting from P10 high pressure spike on P300 shell projectile.

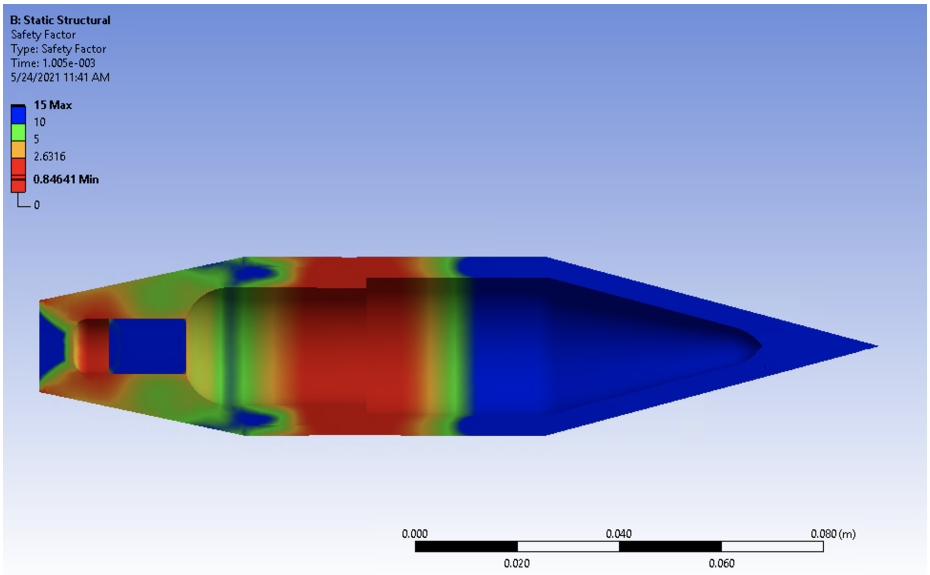

Figure 3.43: Section view of safety factor resulting from P10 high pressure spike on P300 shell projectile.

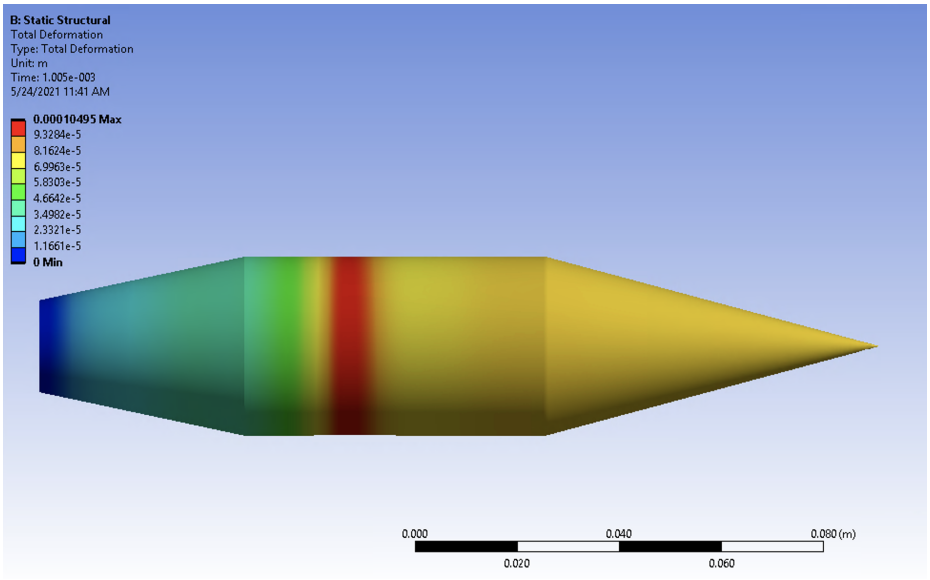

Figure 3.44: Deformation resulting from P10 high pressure spike on P300 shell projectile.

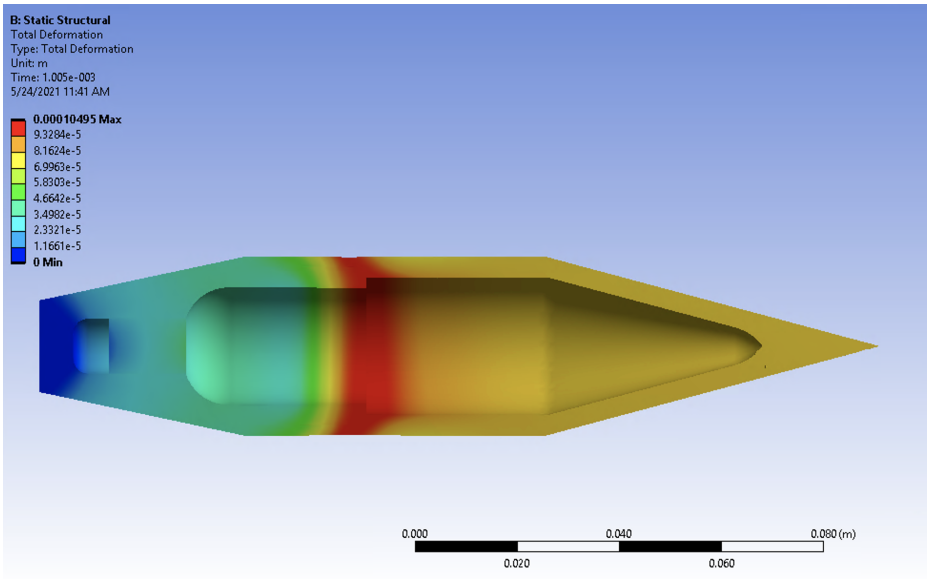

Figure 3.45: Section view of deformation resulting from P10 high pressure spike on P300 shell projectile.

The highest point of the pressure profile from station 10 lies directly over the connection point between the two parts of the projectile. As stated previously, to better encourage simulation convergence the connecting threads were removed and the simulation was done considering the two concentric surfaces to be flat and connected. Naturally the addition of threads would add stress concentrations to the model and possibly reduce the factor of safety thereby compromising the projectile. However, this is only a proposed connection mechanism. These simulation conditions could be emulated if the two pieces were connected with an adhesive or press fit together instead of threaded. Therefore any concerns about the physical modeling being inaccurate on the basis of not simulating the threading can be dismissed.

The projectile was then tested with the pressure profile from the insert. In this case the projectile was constrained by the inside of the cone region on the head of the projectile as there is no volume beneath the shoulder with which to constrain it. The insert pressure profile was again laid over the projectile as seen in Figure 3.24.

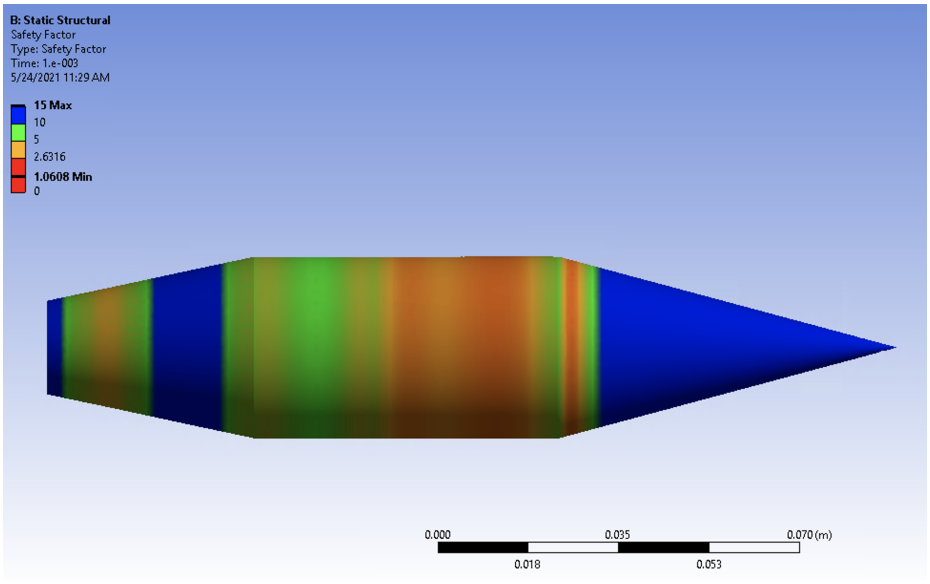

Figure 3.46: Safety factor resulting from Ptrin high pressure spike on P300 shell projectile.

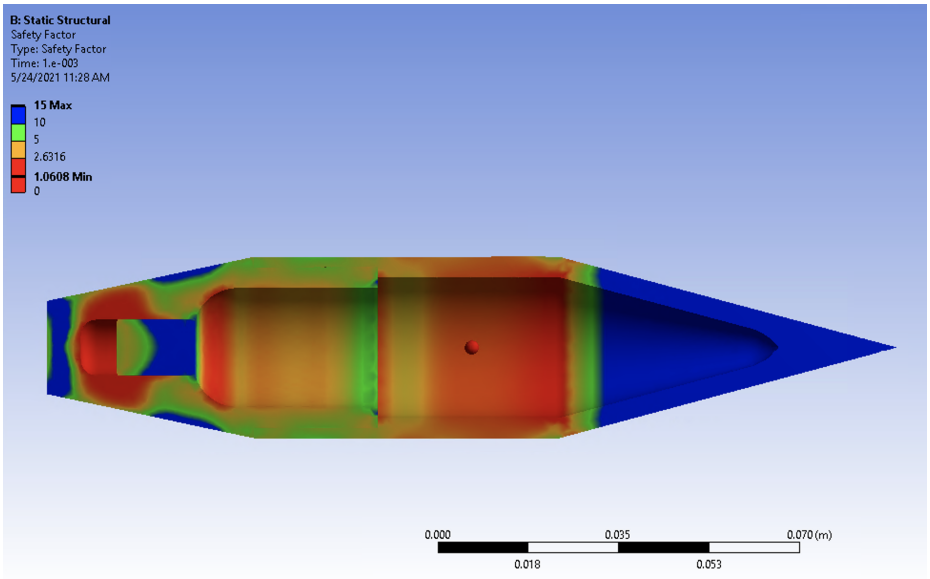

Figure 3.47: Section view of safety factor resulting from Ptrin high pressure spike on P300 shell projectile.

The P300 shell projectile faired better with the pressures at the insert than at Station 10 with the safety factor not dropping below 1 at any point on or within the surfaces. As show by the safety factor in Figures 3.46 and 3.47 and the deformation shown in Figures 3.48 and 3.49 the projectile, while being pushed to its limit in areas, is not yielding or experiencing plastic deformation. These results indicate that the designed P300 7075 aluminum shell projectile can endure high pressures without leading to serious plastic deformation or loss of structural integrity. This suggests that if experiments which exhibited a loss in performance were repeated with the design presented herein, or a similar design, the possibility of projectile deformation causing a loss in performance could be ruled out.

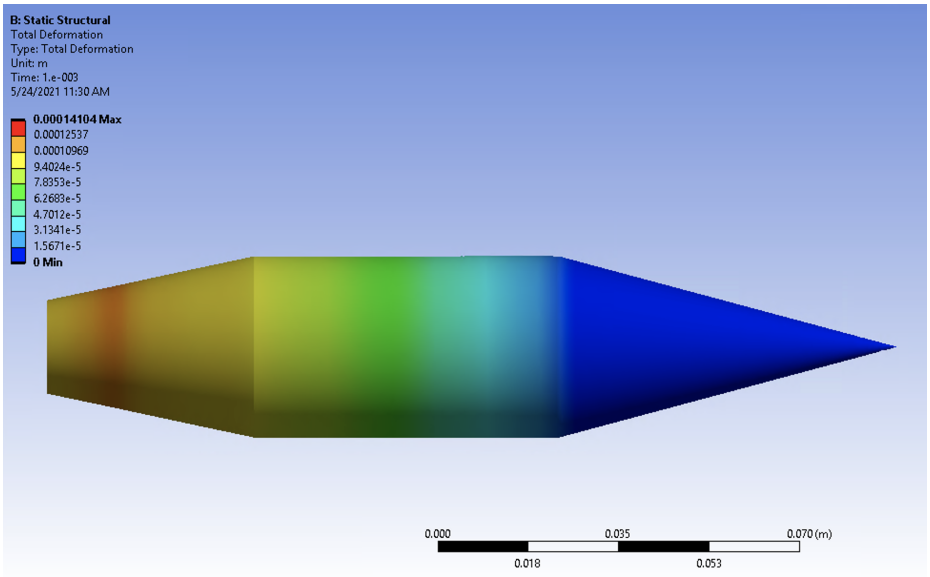

Figure 3.48: Safety factor resulting from Ptrin high pressure spike on P300 shell projectile.

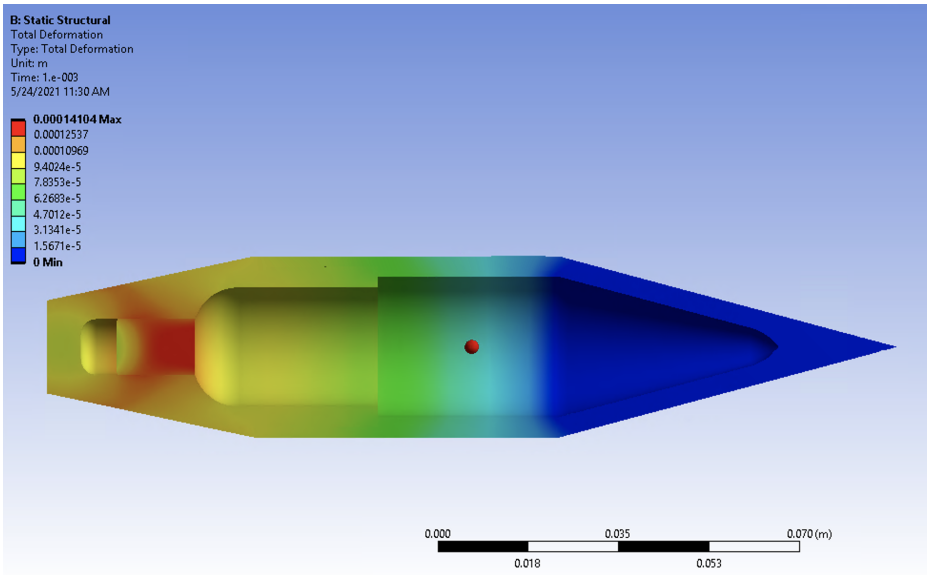

Figure 3.49: Section view of safety factor resulting from Ptrin high pressure spike on P300 shell projectile.

Chapter 4

DISCUSSION

4.1 Synopsis

This experimental investigation took axisymmetric ram accelerator pressure data obtained from in-tube pressure sensors, used magnetic probe information to overlay pressures on projectile surfaces, and simulated the structural effects. It was demonstrated that the polycarbonate P300 projectile does not greatly deform under regular driving pressures; however this was not the case when large pressure spikes occurred in the ram stages. HS2168 served as an example of large pressure spikes in the first ram stage preceding drops in performance in the 2nd stage. Simulated pressure spikes demonstrated that the projectiles used during experimentation experienced plastic deformation both on the surface and internally with the threat of greater deformation shown by large regions of the projectile having a safety factor at or below 1. It is likely that the surface deformation caused by these pressure spikes led to the reduction in performance and therefore if spikes of similar or greater magnitudes are seen during experimentation, the high chance of deformation effecting results must be kept in mind. The design of the baffle tube inserts is such that they are meant to prevent large pressure from overtaking the projectile and causing an unstart. This means that when using baffle tubes it is expected that the tail and body of the projectile will see higher pressures more regularly and the problem of deformation may be prevalent.

Looking to circumvent this problem a 6061 aluminum version of the P300 projectile was then tested under identical pressure loading to determine its structural response. The solid aluminum projectile endured the large pressure during HS2168 better than its polycarbonate counterpart, showing only elastic deformation and a safety factor

above 1 in the relevant regions. However, drawbacks of using the aluminum as a primary projectile lie with its weight. The slightly more than twice as heavy aluminum projectile can not be launched to as high of velocities as the PC, additionally it traverses a smaller velocity range when in the ram stages and as such does not serve as well as a tool for scientific exploration of axisymmetric ram operation.

Problems with projectile weight lead to the third type of projectile tested: the 7075 aluminum shell P300. A 2 part shell style projectile was designed and tested that utilized both a stronger type of aluminum and contained a weight saving cavity. With a weight of 173g with the obturator the helium light gas gun can shoot this projectile up to similar velocity as the polycarbonate projectile. When subjected to the large pressure spikes of HS2168, the shell style projectile maintained external structural integrity with only elastic deformation and safety factors above 1; however, the inside wall of the projectile exhibited small amounts of plastic deformation in the form of stretching slightly in response to the elastic deformation throughout the shell. Considering that the deformation does not affect the flow around the projectile, this projectile style is a strong candidate for being used in future high pressure/velocity studies in order to eliminate the influence of projectile deformation on experimental performance.

Polycarbonate loses almost all of its strength at its glass transition at around 140°C and aluminum becomes half as strong at around 600°C. When exposed to the high combustion temperatures present in ram accelerators it is expected that the projectiles would heat up, begin losing their strength, and thereby be more effected by the large pressure. However, this was an effect not largely considered in this study given the amount of time the projectile spends in the high temperature environment: 4 to 8 milliseconds. When compared to the characteristic thermal diffusion timescales of polycarbonate and aluminum this time is several orders of magnitude lower and therefore thermal effect will be minimal and will not greatly effect the stresses observed. In future experimentation, if the projectile spends longer periods of time in

these environments, thermal effects should be considered both in projectile design and in structural simulation.

4.2 Future Research and Testing

The results presented in this experimental investigation are another step in the development of an optimized projectile. As ram technology continues to develop the challenges will only grow from trying to balance strength and weight to flight stability, payload management, or even someday human transport. In the short term ,extensive testing and research projects can be undertaken to further the study of projectile integrity in the UW ram accelerator.

The natural first step is to take the simulation work that have been done and compare it with experimental data. The Ram Lab has access to a high speed camera as well as a high speed x-ray machine; by inserting several transparent tube sections into the downstream drift tubes one could then image and x-ray the projectile as it passes by. This will allow viewing of both the exterior and interior of the projectile to asses any damage done within the ram section. More information could be gathered by collecting the projectile from the dump tank after each run. Utilizing this setup a series of runs would then be done recreating the conditions of HS2168 and other shots that experienced losses that may have been caused by projectile failure. Depending on the results of the experimental comparison to the FEA that this study presented, a series of CFD analyses could be done using deformed projectile geometries to help determine why exactly this deformation is leading to drops in performance. Through a combination of the simulation work done in this study and future research projects, projectiles can be developed that maximize ram accelerator performance and maintain structural integrity throughout operation. This is a first step not only in advancing scientific study of axisymmetric ram operation, but in developing a ram projectile that will some day be launched to space.

4.3 Conclusion

Using a combination of experimental data and FEA simulation, the structural integrity of 3 projectile configurations were tested. The polycarbonate P300 projectile deforms at pressures measured during experimentation, impacting and reducing performance. Solid 6061-T6 aluminum projectiles are robust to the same pressure levels at the cost of a large increase in weight. To balance these two projectiles attributes, a 2-piece 7075 aluminum shell projectile can be fabricated with a small weight penalty that will be able to endure the high pressures observed during experimentation without deformation. The shell projectile therefore is a strong candidate for use in future high pressure or velocity experimentation.

Bibliography

[1] Brian Dunbar. Advanced space transportation program fact sheet, 2008.

[2] Relly Victoria Petrescu, Raffaella Aversa, Bilal Akash, Filippo Berto, Antonio Apicella, and Florian Ion Tiberiu Petrescu. Project HARP. *Journal of Aircraft and Spacecraft Technology*, 1(4):249–257, 2017.

[3] A. Hertzberg, A. P. Bruckner, and D. W. Bogdanoff. Ram accelerator: A new chemical method for accelerating projectilesto ultrahigh velocities. *AIAA Journal*, 26(2):195–203, 1988.

[4] D. W. Bruckner, A. P. and Knowlen, C. and Hertzberg, A. and Bogdanoff. Ram Accelerator. *Journal of Propulsion and Power*, 7(5):828–836, 1991.

[5] A. J. Higgins, C. Knowlen, and A. P. Bruckner. Ram accelerator operating limits, Part 1: Nature of observed limits. *Journal of Propulsion and Power*, 14(6):959–966, 1998.

[6] A. J. Higgins, C. Knowlen, and A. P. Bruckner. Ram accelerator operating limits, Part 2: Nature of observed limits. *Journal of Propulsion and Power*, 14(6):959–966, 1998.

[7] D. W. Bogdanoff, C. Knowlen, D. Murakami, and I. Stonich. Magnetic detector for projectiles in tubes. *AIAA Journal*, 28(11):1942–1944, 1990.

[8] Carl Knowlen, Navid Daneshvaran, Trever Byrd, and Jesse Dumas. Computational fluid dynamic modeling of baffled tube ram accelerator experiments. *AIAA Aerospace Sciences Meeting, 2018*, (210059):1–11, 2018.

[9] C. Knowlen, J. F. Glusman, R. Grist, A. P. Bruckner, and A. J. Higgins. Experimental investigation of a baffled-tube ram accelerator. *52nd AIAA/SAE/ASEE Joint Propulsion Conference, 2016*, pages 1–10, 2016.

[10] C. Knowlen, T. Byrd, J. Dumas, N. Daneshvaran, J. Glusman, A. P. Bruckner, and A. J. Higgins. Baffled-tube ram accelerator operation with inclined baffles. *53rd AIAA/SAE/ASEE Joint Propulsion Conference, 2017*, (July), 2017.

[11] E. Schultz, C. Knowlen, and A. P. Bruckner. Overview of the subdetonative ram accelerator starting process. *Ram Accelerators*, pages 189–203, 1998.

[12] Timothy Elder. Operation of Polycarbonate Projectiles in the Ram Accelerator. *MSAA Thesis*, 2013.

[13] Thomas Imrich. The Impact of Projectile Geometry on Ram Accelerator Performance. *MSAA Thesis*, 1995.

[14] Trever J Byrd. Experimentally-Driven Model for the Baffled-Tube Ram Accelerator. *MSAA Thesis*, 2018.

[15] Jeffrey F Glusman. Theoretical Performance Model and Initial Experimentation of a Baffled-Tube Ram Accelerator. *MSAA Thesis*, 2016.

[16] Omnexus Material Selection Platform. A Complete Guide to Polycarbonate (PC), 2021.

[17] C. Bundy, C. Knowlen, and A. P. Bruckner. Unsteady effects on ram accelerator operation at elevated fill pressures. *Journal of Propulsion and Power*, 20(5):801–810, 2004.

[18] Pascal Bauer, C. Knowlen, and A. P. Bruckner. Modeling acceleration effects on ram accelerator thrust at high pressure. *Journal of Propulsion and Power*, 21(5):955–958, 2005.

[19] H. W. Liepmann and Anatol Roshko. *Elements of gasdynamics*. Wiley, 1957.

Appendix A

ADDITIONAL FIGURES

Station	Distance from Previous Station [m] (Start of Stage for Station 6)	Distance from Previous Station [in] (Start of Stage for Station 6)
6	0.3036	11.95
7	0.3571	14.06
8	0.3571	14.06
9	0.3571	14.06
10	0.3571	14.06
Spacer Insert	0.2846	11.20
11	0.3219	12.67
12	0.3571	14.06
13	0.3571	14.06
14	0.3571	14.06
15	0.3571	14.06

Figure A.1: Dimensions between each of the stations along the ram test section.

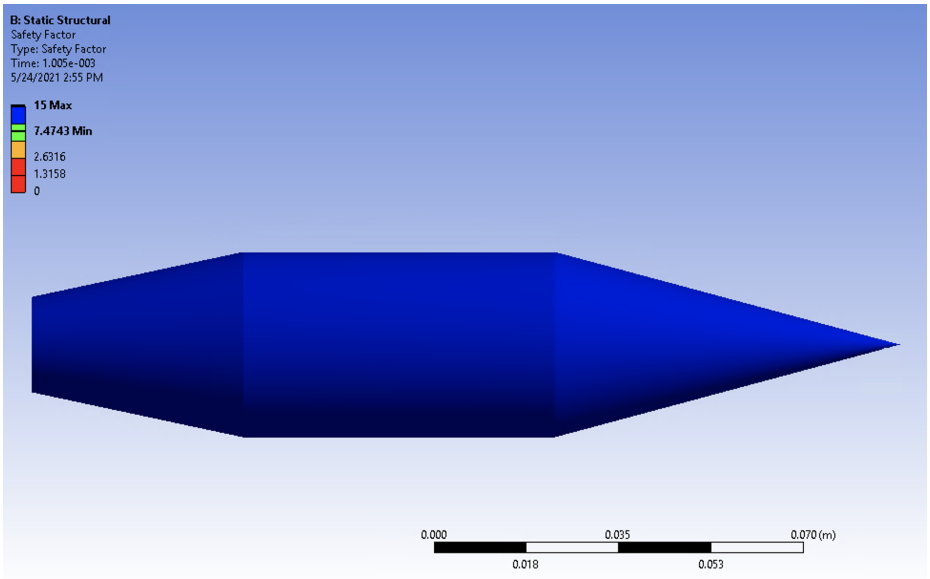

Figure A.2: Safety factor resulting from P13 on P300 shell projectile.

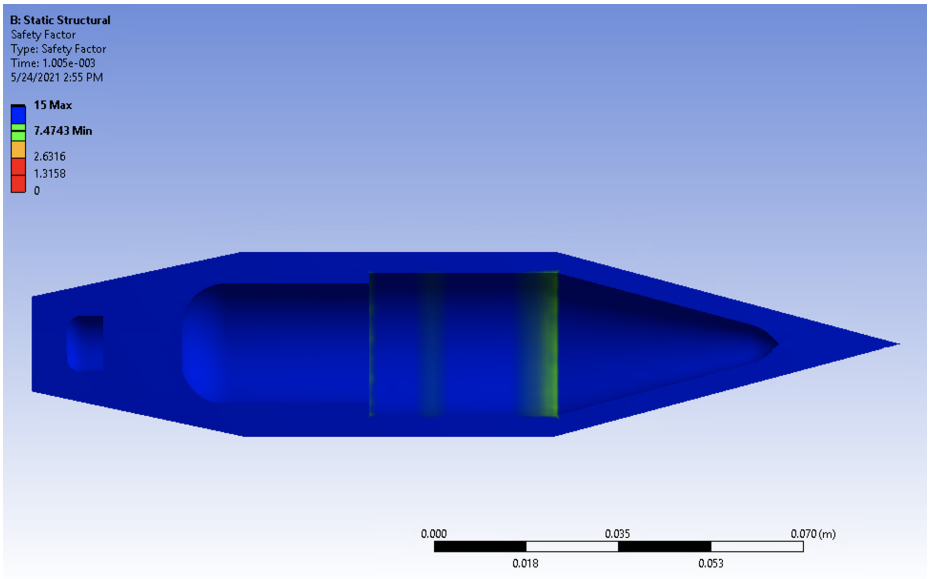

Figure A.3: Section view of safety factor resulting from P13 on P300 shell projectile.

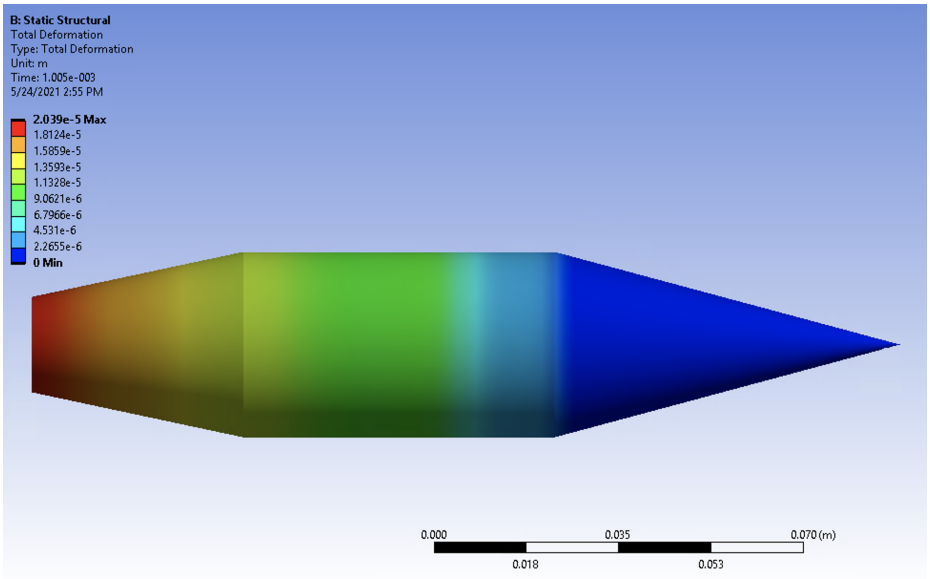

Figure A.4: Deformation resulting from P13 on P300 shell projectile.

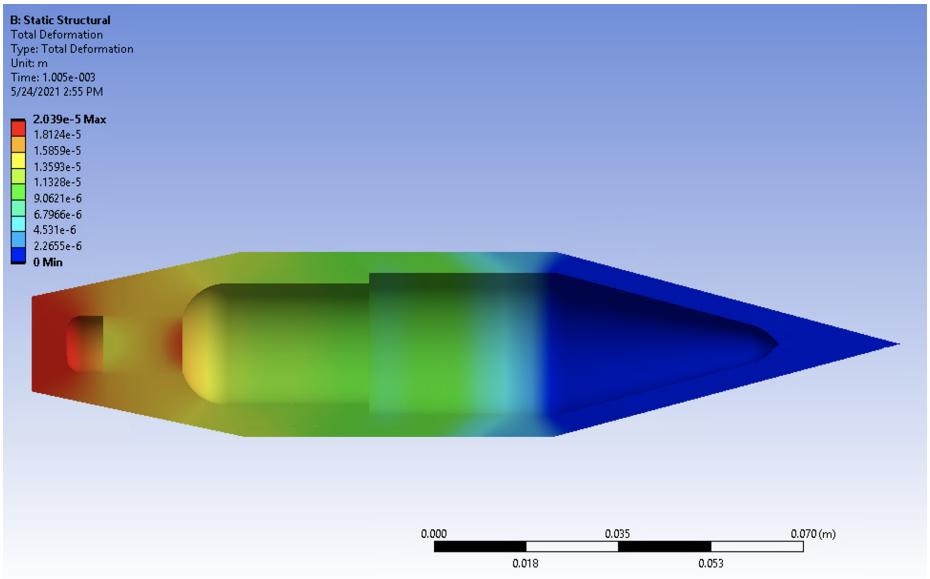

Figure A.5: Section view of deformation resulting from P13 on P300 shell projectile.

Appendix B

MATERIAL INFORMATION

GABRIAN
INTERNATIONAL(H.K.) LTD

6061 Aluminum Alloy: Properties

General Characteristics

Characteristic	Appraisal
Strength	Medium to High
Corrosion Resistance	Good
Weldability & Brazability	Good
Workability	Good
Machinability	Good

Chemical Composition

Element	Minimum %	Maximum %
Magnesium	0.8	1.2
Silicon	0.4	0.8
Iron	No Min	0.7
Copper	0.15	0.4
Manganese	No Min	0.15
Chromium	0.04	0.35
Zinc	No Min	0.25
Titanium	No Min	0.15
Other Elements	No Min	0.05 each, 0.15 in total

Physical Properties

Property	6061-T4	6061-T6
Density	2.70 g/cc | 0.0975 lb/in³	2.70 g/cc | 0.0975 lb/in³

Mechanical Properties

Property	6061-T4	6061-T6
Tensile Strength	241 MPa | 35000 psi	310 MPa | 45000 psi
Yield Strength	145 MPa | 21000 psi	276 MPa | 40000 psi
Modulus of Elasticity	68.9 GPa | 10000 ksi	68.9 GPa | 10000 ksi

Thermal Properties

Property	6061-T4	6061-T6
Coefficient of Thermal Expansion @ 20.0 - 100 °C Temp	23.6 µm/m-°C | 13.1 µin/in-°F	23.6 µm/m-°C | 13.1 µin/in-°F
Thermal Conductivity	154 W/m-K | 1070 BTU-in/hr-ft²-°F	167 W/m-K | 1160 BTU-in/hr-ft²-°F

Gabrian International (H.K.) Ltd. +1 (603) 749-1995 https://www.gabrian.com

Figure B.1: 6061-T6 Aluminum Properties, information provided by Gabrain International Ltd.

GABRIAN
INTERNATIONAL(H.K.) LTD

7075 Aluminum Alloy: Properties

General Characteristics

Characteristic	Appraisal
Strength	High
Corrosion Resistance	Average
Weldability & Brazability	Poor
Workability	Poor
Machinability	Fair

Chemical Composition

Element	Minimum %	Maximum %
Silicon	No Min	0.4
Iron	No Min	0.5
Copper	1.2	2
Manganese	No Min	0.3
Magnesium	2.1	2.9
Chromium	0.18	2
Zinc	5.1	6.1
Titanium	No Min	0.2
Other Elements	No Min	0.05 each, 0.15 in total

Physical Properties

Property	7075-O	7075-T6, -T651	7075-T73, -T7351
Density	2.81 g/cc | 0.102 lb/in³	2.81 g/cc | 0.102 lb/in³	2.81 g/cc | 0.102 lb/in³

Mechanical Properties

Property	7075-O	7075-T6, -T651	7075-T73, -T7351
Tensile Strength	228 MPa | 33000 psi	572 MPa | 83000 psi	505 MPa| 73200 psi
Yield Strength	103 MPa | 15000 psi	503 MPa | 73000 psi	435 MPa | 63100 psi
Modulus of Elasticity	71.7 GPa | 10400 ksi	71.7 GPa | 10400 ksi	72.0 GPa | 10400 ksi

Thermal Properties

Property	7075-O	7075-T6, -T651	7075-T73, -T7351
Coefficient of Thermal Expansion @ 20.0 - 100 °C Temp	23.4 µm/m-°C | 13.0 µin/in-°F	23.4 µm/m-°C | 13.0 µin/in-°F	23.4 µm/m-°C | 13.0 µin/in-°F
Thermal Conductivity	173 W/m-K | 1200 BTU-in/hr-ft²-°F	0.960 J/g-°C | 0.229 BTU/lb-°F	155 W/m-K | 1080 BTU-in/hr-ft²-°F

Gabrian International (H.K.) Ltd. +1 (603) 749-1995 https://www.gabrian.com

Figure B.2: 7075-T6 Aluminum Properties, information provided by Gabrain International Ltd.

Appendix C

MATLAB CODE

```
clear all
close all
clc
% For Use with RTRA 200 Configurations (CS98+,HS2116+)
%Change filename to the shot folder
%HS2215 is example of good lower pressure spike started shot
%HS2214 is example of a high pressure spike unstart
%HS2159 is a solid driving railed shot
%HS2168 is random reduced return in rail stage THIS SHOT IS
    THE ONE!
filename = 'HS2159';
%Change to number of samples from Labview input
%num_samples = 50000;
%sample_rate=1.25e6;
%Change test section station numbers for final pressure plot
test_section=6:10;
calibration=1;
%% NO NEED TO CHANGE ANYTHING BELOW HERE :)
disp('JG 7/15/16 & TB 11/10/17 & BL 8/12/19');
%% Data procurement from LABview output file and
    Instrumentation Log
%creates color scheme of most diverse colors
```

```
colors=distinguishable_colors(10);
colors(4,:)=[]; colors(6,:)=[];
%moves directory into the folder of the shot name
cd(filename);
fid = fopen(filename);
A = textscan(fid,'%f','headerlines',23);
num_samples = length(A{1})/33;
%creates matrix of data
big_data = reshape(A{1},33,num_samples)';
sample_rate = num_samples/big_data(end,1);
%creates matrix of data
big_data = reshape(A{1},33,num_samples)';
%this file must exist within the shot file
loadstring=['Instrument Log_' filename '.xlsx'];
%DAS Modules setup
[num,textin]=xlsread(loadstring,'I21:P24');
%MAG Strings
[magnum,magtext]=xlsread(loadstring,'I4:P9');
%Calibration data
[pcalnum,pcalname]=xlsread(loadstring,'S5:T50');
%Probe positions
[i_pcalnum,i_pcalname]=xlsread(loadstring,'F3:F46');
fclose(fid);
cd ..

%% Creation of arrays and indexing of Mag and Pressures
i_pcalname(1)=[]; %getting rid of 'Cable' from beginning of
```

```
    string and to guarantee no dropped values
pnums=1:42; %all possible stations
for j=1:length(pnums)
pressure{j}=['P' num2str(pnums(j))]; %adding P in front as to
    match instrumentation log
end
%% pressure=['PLt' pressure]'; %adding in PLt to possible
    pressure locations
pressure=['PLt' 'PRTIN' pressure]'; %adding in PLt to
    possible pressure locations
%% magnet={'Ma' 'Mb' 'Mc' 'Md' 'Me' 'Mf'}; %create all mag
    string possibilities
magnet={'Ma' 'Mb' 'Mc' 'Md' 'Me' 'Mf'}; %create all mag
    string possibilities
for j=1:length(i_pcalname)
    %array of calibrated probles next to all possible P
        locations
    pressure{j,2}=i_pcalname{j};
end
for j=1:length(magnet)
    %Finds the matrix locations of where magstrings are
        located in the DAS
    dummy1=find(strcmp(magnet{j},textin));
    if isempty(dummy1) % Checks to see if the general "magnet
        " array has too many inputs
        dummy2 = magnet;
        magnet = dummy2(1:j-1); % Replace the general magnet
```

```
            array with the correct one
66          break % End for loop
67      else
68          index_mag(j)=dummy1;
69      end
70  end
71  jj=0;
72  mask=[0:7;8:15;16:23;24:31]; %match DAS input numbers (
    entered to get data)
73  for j=1:length(pressure)
74      %find which pressure locations are being used and where
        to create an
75      %array of used values (index_pressure) and their
        calibration data
76      index_check=find(strcmp(pressure{j,1},textin));
77      if ~isempty(index_check)
78          jj=jj+1;
79          index_pressure(jj,1)=find(strcmp(pressure{j,1},textin
            ));
80          plot_pressure{jj}=pressure{j};
81  %           pressure{jj,3}=.09;
82          if ~isempty(pressure{j,2})
83              index_cal=find(strcmp(pressure{j,2},pcalname));
84              pressure{j,3}=pcalnum(index_cal);
85          else
86              pressure{j,3}=.09;
87          end
```

```
88            pressure{j,4}=index_pressure(jj);
89            pressure{j,5}=mask(pressure{j,4});
90        end
91    end
92    %index_pressure(index_pressure(:,2)==0,2)=.09; %Nominal value
93    %mask=[0:7;8:15;16:23;24:31]; %match DAS input numbers (
          entered to get data)
94    masked_mag=mask(index_mag); %mag inputs for DAS
95    for j=1:length(pressure)
96        if ~isempty(pressure{j,5})
97            if calibration==1
98                %big_data(:,pressure{j,5})=big_data(:,pressure{j
                      ,5})/pressure{j,3};
99                big_data(:,pressure{j,5})=big_data(:,pressure{j
                      ,5})./0.0001;
100           end
101       end
102   end
103   masked_pressure=[pressure{:,5}];
104   %masked_pressure;
105   big_data(:,1)=1000*big_data(:,1); % converting seconds to
          milliseconds
106
107   %%%%%%%%%CHASE'S PROJECTILE DATA EXTRACTION SECTION
          !!!!!%%%%%%%%%
108
109   probe_ref = 18; %This is the reference column in big data for
```

```
    P13, HS2214
tm = 21.618./1000; %Magnet Time at P13 in sec, input from
    sheet
vel = (1058+1089)./2; %Velocity at Station P13 in m/s,
    average of speeds on either side of P7
t0 = (1./vel).*(vel.*tm - (4.737.*0.0254)); %Time of tip in
    seconds
t1 = (1./vel).*(vel.*tm + (1.740.*0.0254)); %Time of tail in
    seconds
t_tot = t1 - t0; %Time from tip to tail in seconds
dt = (8e-4)./1000; %Time step in seconds
nstep = round(t_tot./dt); %Number of recorded pressure values
    over the body
proj_length = 6.477.*0.0254; %projectile length in meters
dx = proj_length./nstep;
chase_data = zeros(nstep,2);
foundit = 0;
for i = 1:length(big_data(:,1)) %Iterate through array to
    identify start of the projectile
    if(abs((t0.*1000) - big_data(i,1)) < 8e-4) %We have found
        the projectile!
        for j = 1:nstep %Save distance along projectile and
            pressure value
            chase_data(j,1) = j.*dx; %Position
            chase_data(j,2) = abs(big_data(i+j,probe_ref)); %
                Pressure
        end
```

```
127             foundit = 1;
128         end
129         if(foundit)
130             break;
131         end
132     end
133     writematrix(chase_data,'CHASE_HS2159_P13.csv') %turn on when
        writing out
134     %%%%%%%%%%%%%%%%%%%%%%%%%%%%%%%%%%%%%%%%%%%%%%%%%%%%%%%%%%%%
135
136     %% Plotting of Mag and Pressure data for all given stations
137     for j=length(masked_pressure):-1:1
138         f=figure;
139         for jj=1:length(masked_mag)
140             %Plot Mag data normalized by the absolute maximum
                voltage
141             plot(big_data(:,1),big_data(:,masked_mag(jj)+2)/max(
                abs(big_data(:,masked_mag(jj)+2))),'Color',colors(
                jj,:));
142             hold on
143         end
144         %Plot calibrated pressure data
145         plot(big_data(:,1),big_data(:,masked_pressure(j)+2),'
            Color',colors(jj+2,:),'LineWidth',1.2);
146         hold off
147         title(plot_pressure{j})
148
```

```
149     disp(['plotting: ',plot_pressure(j)]) %added for chase to
            figure out big_data
150     ref_input = (masked_pressure(j)+2);
151     disp(ref_input) %added for chase
152     disp('...')
153
154     %Changes name of plot in the windows system
155     set(f,'name',plot_pressure{j},'numbertitle','off')
156     xlabel('Time (ms)')
157     if calibration==1
158         ylabel('Pressure (psi) | Normalized Mag Response')
159     else
160         ylabel('Uncalibrated Pressure | Normalized Mag
              Response')
161     end
162 % %     legend('Ma','Mb','Mc','Md','Me','Mf','Pressure Data
    ','Location','SouthEast');
163     legend('Ma','Mb','Mc','Pressure Data','Location','
          SouthEast');
164 end
165 %% Holds the plots while user inputs data into New BT Data
166 input=menu('Click data saved button when finished inputting
    data into NEW BT DATA, Exit to end program, or individual
    plots.','Data Saved - Plot Pressure with Mags','Exit
    Program','Plot Individual Data Inputs');
167 switch input
168     case 1
```

```
169     case 2
170         disp('Code has been terminated by user.')
171     case 3
172         close all
173         plots= [masked_mag,masked_pressure];
174         titles= [magnet,plot_pressure];
175         for j=length(plots):-1:1
176             port_num=plots(j);
177             f=figure;
178             plot(big_data(:,1),big_data(:,port_num+2))
179             title(titles{j})
180             set(f,'name',titles{j},'numbertitle','off')
181 
182             % Adjust cursor time data to have 5 digits of
                    precision (can adjust
183             % further by modifying "cursor_data_precision.m".
                    - BL
184             dcmObj = datacursormode; % Turn on data cursors
                    and return object
185             set(dcmObj, 'UpdateFcn', @data_cursor_precision);
                    % Tells the data cursor to use "
                    cursor_data_precision.m" instead of default
186             % Must have "cursor_data_precision.m" in folder
187 
188         end
189         figure
190         plot(big_data(:,1),(big_data(:,7)))
```

```
191         title('Station 9')
192         xlabel('Time(ms)')
193         ylabel('Semi-Log Light Intensity')
194         hold on
195         plot(big_data(:,1),-35*big_data(:,17))
196         yyaxis right
197         ylabel('Uncalibrated Pressure')
198         legend('Semi-Log Luminous Intensity','Uncalibrated
               Pressure')
199         hold off
200         input=menu('Click Data Saved when finished inputting
               data into NEW BT DATA.','Data Saved - Plot
               Pressure with Mags','Exit Program');
201         switch input
202             case 1
203             case 2
204                 disp('Code has been terminated by user.')
205         end
206 end
207
208 %%% Creates Pressure plots with mag references based on New
      BT Data inputs
209 close all
210
211 loadstring='New BT Data 6-15-2017.xlsm';
212 %Only saves the first mag and pressure time
213 [num2,magnames]=xlsread(loadstring,filename,'C32:J72');
```

```
214 num2(isnan(num2))=0; %turns blanks into zeros
215 num2(:,[1,2,3,5,6,7])=[]; %gets rid of mag-2 pres
    b4correction
216 %num2=num2*.001; %converts to seconds
217 num2(end,:)=[];
218 magnames(:,[1,3:end])=[];
219
220 pnum2=find(num2(:,2)~=0);%finds places pressure data is
    recorded
221 %pnum2=num(val,3);%saves station numbers for those specific
    pressure locations
222 pnum2=pnum2-1;
223 for j=1:length(pnum2)
224     pressure2{j}=['P' num2str(pnum2(j))]; %Creates pressure
        station names
225     if find(strcmp(pressure2{j},'P0'))== 1;
226         pressure2{j}='PLt'; %if P0 exists, it is PLt
227     end
228 end
229 pressure2=pressure2';
230 for j=1:length(pressure2)
231     ind_p(j,1)=find(strcmp(pressure2{j},pressure));
232 end
233 clear pressure2
234 pressure2{j,:}=pressure(ind_p,:);
235 pressure2=pressure2{end,1};
236 % jj=0;
```

```
237 % for j=1:length(pressure2)
238 %     %find which pressure locations are being used and where
        to create an
239 %     %array of used values (index_pressure) and their
      calibration data
240 %     index_check=find(strcmp(pressure2{j,1},textin));
241 %     if ~isempty(index_check)
242 %         jj=jj+1;
243 %         index_pressure2(jj,1)=find(strcmp(pressure2{j,1},
      textin));
244 %         plot_pressure2{jj}=pressure2{j,1};
245 %         if ~isempty(pressure2{j,3})
246 %             index_cal2=find(strcmp(pressure2{j,3},pcalname)
      );
247 %             index_pressure2(jj,2)=pcalnum(index_cal2);
248 %         end
249 %     end
250 % end
251 % index_pressure2(index_pressure2(:,2)==0,2)=.09; %Nominal
      value if no calibration data
252 % masked_pressure2=mask(index_pressure2(:,1));
253 num2=num2(pnum2+1,:);
254 pindex=floor(num2(:,2)*sample_rate/1000);
255 deltime=floor(200e-6*sample_rate);
256 if exist([filename '/Images'],'dir') ~= 7
257     mkdir([filename '/Images']);
258 end
```

```
259
260 index_pressure2=[pressure2{:,5}];
261 for j=1:length(index_pressure2)
262     f=figure;
263     set(f,'name',pressure2{j,1},'numbertitle','off')
264     indices=pindex(j)-deltime:pindex(j)+4*deltime;
265     %if num2(j,1)*sample_rate < pindex(j)+4*deltime
266         plot(big_data(indices,1),big_data(indices,pressure2{j
                ,5}+2))
267         minp=min(big_data(indices,pressure2{j,5}+2));
268         maxp=max(big_data(indices,pressure2{j,5}+2));
269 %       else
270 %           mag=floor(num2(j,1)*sample_rate);
271 %           plot(big_data(pindex(j)-deltime:mag+3*deltime,1),
    index_pressure2(j,2)*big_data(pindex(j)-deltime:mag+3*
    deltime,masked_pressure2(j)+2))
272 %           minp=min(index_pressure2(j,2)*big_data(pindex(j)-
    deltime:mag+3*deltime,masked_pressure2(j)+2));
273 %           maxp=max(index_pressure2(j,2)*big_data(pindex(j)-
    deltime:mag+3*deltime,masked_pressure2(j)+2));
274 %       end
275     title(pressure2{j,1})
276
277     if num2(j,1)==0
278         title([pressure2{j,1} ' - No Mag at Station'])
279     else
280         hold on
```

```
281             plot([num2(j,1),num2(j,1)],[minp,maxp],'m')
282             title(pressure2(j,1))
283         end
284         xlabel('Time (ms)')
285         if calibration==1
286             ylabel('Calibrated Pressure (psi)')
287         else
288             ylabel('Uncalibrated Pressure')
289         end
290         cd(filename)
291         cd('Images')
292         saveas(gcf,[filename '_' pressure2{j,1}],'png');
293         cd ..
294         cd ..
295     end
296
297
298     for j=1:length(test_section)
299         pressure3{j}=['P' num2str(test_section(j))]; %Creates
                pressure station names
300     end
301     for j=1:length(pressure3)
302         ind_p2(j,1)=find(strcmp(pressure3{j},pressure));
303     end
304     clear pressure3
305     pressure3{j,:}=pressure(ind_p2,:);
306     pressure3=pressure3{end,1};
```

```
307 test_section_pnum=pnum2( pnum2>= test_section(1) & pnum2 <=
        test_section(end));
308
309
310 %indices=pindex(test_section_pnum(1)-1)-deltime:pindex(
        test_section_pnum(end)-1)+5*deltime;
311 indices = 10625:15001;
312 %indices=8751:12511;
313 f=figure;
314 set(f,'name','Pressure Plot','numbertitle','off')
315
316 for j=1:length(test_section_pnum)
317     plot(big_data(indices,1),test_section_pnum(j)+big_data(
            indices,pressure3{test_section_pnum(j)-5,5}+2),'Color',
            colors(j,:))
318     hold on
319 end
320 xlabel('Time (ms)','FontSize',18); ylabel('Station Number','
        FontSize',18)
321 title([filename ' Test Section Pressure Plots'],'FontSize'
        ,18)
322 grid on
323 cd(filename)
324 cd('Images')
325 saveas(gcf,[filename '_Pressures'],'png');
326 cd ..
327 cd ..
```

```
328 cd 'Pressure Plots'
329 saveas(gcf,[filename '_Pressures'],'png');
330 cd ..
331
332
333
334 display('4 8 15 16 36 42')
335 display('Done')
```